Title	Estimating streamflow of the Abashiri River under likely future climate and land use land cover conditions
Author(s)	史, 穆清
Degree Grantor	北海道大学
Degree Name	博士(環境科学)
Dissertation Number	甲第15266号
Issue Date	2023-03-23
DOI	https://doi.org/10.14943/doctoral.k15266
Doc URL	https://hdl.handle.net/2115/89635
Type	doctoral thesis
File Information	Shi_Muqing.pdf

Ph.D. Dissertation

Estimating streamflow of the Abashiri River under likely future climate and land use land cover conditions

(将来起こりうる気候と土地利用・土地被覆変化による網走川の流出推定)

Graduate School of Environmental Science,

Hokkaido University

Shi Muqing

February 2023

Abstract

It has become better known in recent years that climate and land use land cover (LULC) changes can significantly impact local streamflow behaviors. Therefore, studies on estimating future streamflow behaviors in response to such changes have become abundant in recent years. However, more efforts have been dedicated to improving the robustness of future climate and LULC projections. In contrast, the representation of hydrological processes in the river basin needs to be more noticed and adequate. More specifically, the application of the most widely used tool under this topic, the physical hydrological model, is often met with two major issues that may render the entire estimation unreliable: data limitation, and the use of statistical tuning. Due to the commonly large number of parameters in hydrological models, both issues are generally inevitable in actual practices, which is why minimizing the use of tuning under limited data availability is a necessary and meaningful notion. However, the practicality and significance of this notion have yet to be adequately explored. Therefore, this study aims to estimate the future streamflow of the Abashiri River basin (ARB) under likely climate and LULC conditions while fulfilling the notion. A consistent and physically meaningful approach was proposed and realized in a hydrological distributed model, Soil and Water Assessment Tool (SWAT), by primarily relying on open-access resources in response to the data limitation in this study. ARB was selected as the study site mainly due to its local significance of streamflow to the active and stable fishery activities in Lake Abashiri, in addition to the growing concerns by the local stakeholders regarding the stability of river flow in the future.

The future climate change projection was obtained from the Japan Meteorological Agency Regional Climate Projection Data for Japan, which was projected using a non-hydrostatic regional climate model under IPCC RCP2.6 and RCP8.5 scenarios in 2076-2095. Under the future climate conditions, major changes in streamflow include a significant change in the timing and quantity in the melting season, and a significant decrease in the low flows. Mixed impacts of significantly decreased winter precipitation and increased temperature led to a clear difference in the change of winter streamflow between the two scenarios. Significant implications include an increased risk of irrigation water shortage in the early summer and a less stable condition for fishery activities in Lake Abashiri. The future LULC projection was obtained from a vegetation survey-based dataset developed by the Predicting and Assessing Natural Capital and Ecosystem Services project. The projection was made as of 2050, focusing mainly on the future development directions of the natural capital source, and population distribution. Under the future LULC conditions, quantitatively insignificant forest change led to a slight general decrease in streamflow. On the other hand, the significant relative difference in paddy field led to a significant difference of change in future streamflow from midsummer to autumn. From these results, it was implied that future LULC in the ARB may affect streamflow less significantly than the impact from climate, while concern for irrigation water use may be raised. In addition to the streamflow estimation results, this study successfully demonstrates the practicality and necessity of minimizing the use of tuning in SWAT under a data limitation, and emphasizes the significance of physically meaningful sophistication for SWAT in a predictive application as the present study.

Contents

1. Introduction

Streamflow is an essential component of the continental water processes, and its variation is influenced by climate and the nature of the land surface (Brutsaert, 2005; Haines et al., 1988). Climate change could impact streamflow through the change in precipitation and evaporation (e.g., Barnett et al., 2005; Croitoru & Minea, 2015; Tan & Gan, 2015; van Vliet et al., 2013) and the change on the land surface, or in most cases, land use land cover (LULC) change, could impact the streamflow through changes in surface runoff, evaporation, or the variation in the groundwater storage (e.g., Schilling et al., 2008; Turner et al., 1995; Twine et al., 2004; Wang et al., 2017). Climate and LULC changes are generally considered the major driving factors for the change in streamflow (Wang et al., 2020). To quantitatively clarify the relationship between the two factors and streamflow, three different techniques are widely used: (1) paired catchment analysis (e.g., Bosch & Hewlett, 1982; Brown et al., 2005; Changnon & Demissie, 1996; Zhao et al., 2010); (2) statistics-based analysis (e.g., Bulygina et al., 2011; Costa et al., 2003; López-Moreno et al., 2006; Zheng et al., 2016); and (3) physical hydrological modeling (e.g., Kiros et al., 2015; Li et al., 2012; Ward et al., 2008). Particularly in the case of predicting such a relationship, physical complexity, partitioning on the sources of impact, and spatiotemporal scale, are the three crucial points to the reliability of streamflow estimations (Bulygina et al., 2013; Ludwig et al., 2009; Sivapalan, 2003; Wang et al., 2020). Therefore, the hydrological model is often considered the preferable tool in estimating future streamflow in response to the climate and LULC changes, as it can accommodate the three key points better than the other techniques on principle.

Hydrological models can generally be categorized into two types, i.e., the lumped model, in which the river basin is considered as a whole and the spatial heterogeneity is therefore neglected, and the distributed model, which divides the river basin into subbasin-level compositions, and takes many aspects including topography, LULC, and soil conditions into account (Japan Society of Civil Engineers, 2019). Both the lumped model (e.g., Tan & Gan, 2015; Wang et al., 2017) and distributed model (e.g., Aich et al., 2014; Lahmer et al., 2001; Schilling et al., 2008; Twine et al., 2004) have been utilized in previous studies of the same topic. Nevertheless, because the distributed model better consolidates the three crucial reliability points in streamflow estimations than the lumped models, the former is more frequently used in recent studies. Distributed models can give rise to a better understanding of the complex interplays in the realistic river system, provided their numerical parameters can be determined appropriately (Brutsaert, 2005). However, two significant issues are subsumed under this requirement due to the commonly large number of parameters in the hydrological models, i.e., the data limitation and the use of statistical tuning (Brutsaert, 2005; Hamilton, 2007). Producing reliable streamflow estimations using a hydrological model under limited data availability is, therefore, a challenging and necessary research target, especially considering that the misuse and overuse of statistical tuning have become frequently overlooked issues in recent studies (Abbaspour, 2022). Data limitation and the use of statistical tuning are generally interconnected, and while the former is primarily exogenous, the latter may be practically minimized. Minimizing the use of tuning in hydrological modeling is not an unprecedented notion, but its practicality and significance under a data limitation are yet to be adequately explored. In this study, a consistent and physically meaningful approach with the aim of minimizing the use of tuning in a hydrological distributed model was proposed and realized, which is then utilized for the estimation of future streamflow under a series of future climate and LULC conditions. The study was conducted in the Abashiri River basin, Hokkaido, Japan, the selection of which is discussed in chapter 2. The future conditions are introduced in chapter 3, and used as the boundary conditions for the streamflow simulation in the distributed model, Soil and Water Assessment Tool (SWAT), the detail of which are described in chapter 4. Estimated future streamflow and its interpretation are discussed in chapter 5. Discussion on the significance and remaining limitations are presented in chapter 6. Conclusions are summarized in chapter 7.

2. Study site

The Abashiri River basin (ARB) is located in northeastern Hokkaido, northern Japan, 44°1′22″N 144°16′30″E (Fig. 1). The main channel is approximately 115 km, and the basin area is about 1,380 km^2. It originates in the Akan Mountain Range and flows through Tsubetsu Town and Bihoro Town, where the two major tributaries, i.e., Tsubetsu River and Bihoro River, join the main channel, respectively. The river then flows into Lake Abashiri, a eutrophic brackish lake with a mean elevation of around 0 m.s.l., a surface area of 32 km^2, and a maximum water depth of 16 m (Nakajima et al., 2004). Seawater intrusion is frequent in Lake Abashiri. As a result, this study only estimate streamflow above the lake. Once out of the lake, the river passes through Abashiri City and enters the Sea of Okhotsk. Additionally, river management constructions (e.g., weir, levee, revetment) in the main channel and major tributaries have been conducted since the 1950s (Hokkaido Regional Development Bureau, 1994). Red triangles in Fig. 1 denote the location of river observation stations established by the Abashiri Development and Construction Department, Ministry of Land, Infrastructure, Transport and Tourism (MLIT). Observed daily streamflow data from the four stations were used in this study, obtained from the Water Information System of MLIT (http://www1.river.go.jp/).

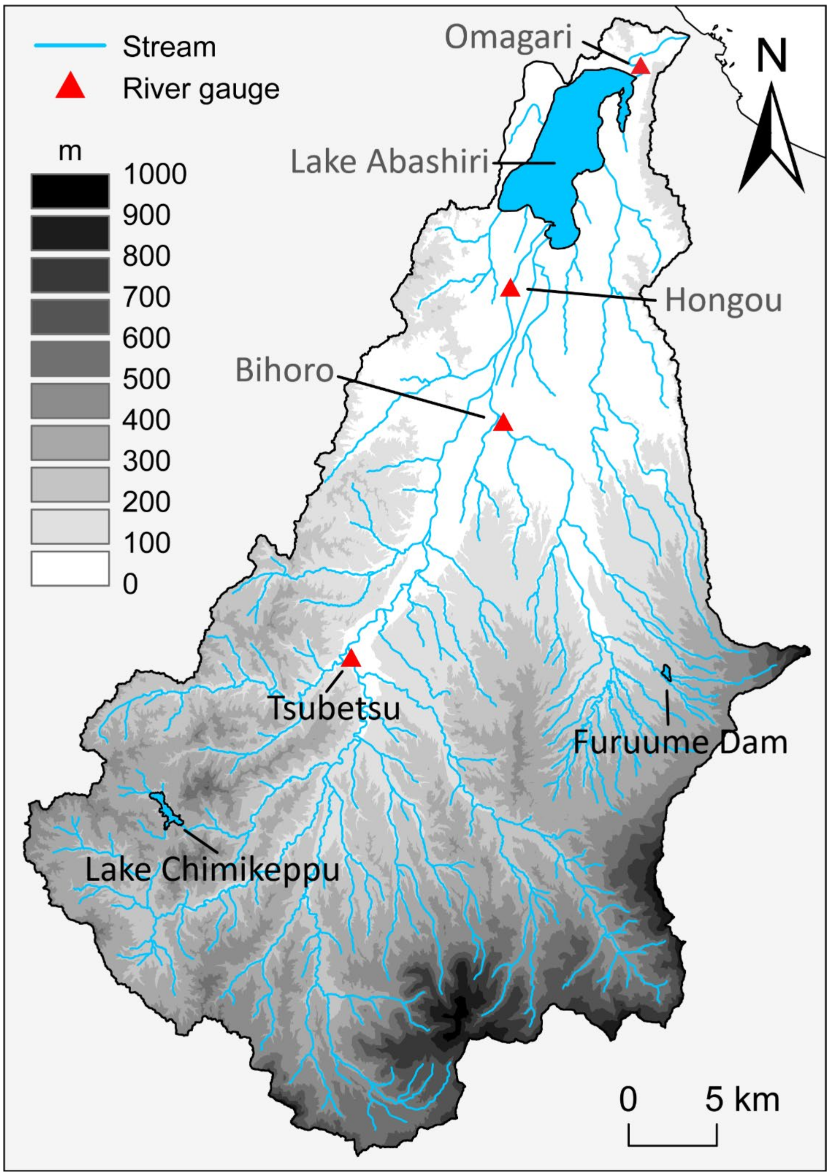

Fig. 1. River network, elevation variation, streamflow stations, and major water bodies in the ARB.

The climate in this region is classified as the Okhotsk Sea-side type, which typically includes low precipitation, extensive diurnal temperature range, cool summer, and severely cold winter. According to the Japan Metrological Agency (JMA) observation records (https://www.data.jma.go.jp/obd/stats/etrn/index.php), the annual mean precipitation in this region is the lowest in Japan (778.6 mm at Bihoro Town in 1991-2020). The annual mean temperature was 5.8 °C, varying from 0.1 °C to 11.6 °C from 1991-2020. While foehn wind during spring could lead to sudden temperature rise and increase of precipitable water vapor (Mori & Sato, 2014), the cold and moist air caused by the Okhotsk High leads to a generally low temperature and frequently but weak precipitation during spring and summer. Precipitation and temperature exhibit relatively higher variabilities during autumn when precipitation reaches its highest level of the year. In winter, the drift ice in the Sea of Okhotsk reduces the water vapor over the sea surface, leading to lower precipitation and a more likely temperature drop. The middle-stream region of the ARB is largely covered by cropland, and the major crops include sugar beet, wheat, potato, and onion (9,430 ha, 8,013 ha, 6,761 ha, and 1,128 ha, respectively in 1993-2004). Even though the coverage of the paddy field is much smaller in comparison (956 ha in 1993-2004), the water taken from the river channel for irrigation use has been chiefly contributed to the paddy field rather than the other crops (Hokkaido Regional Development Bureau, 1994). The upper-stream region is mostly covered by forest, which mainly includes Japanese oak (*Quercus crispula*), Japanese lime (*Tilia japonica*), painted maple (*Acer pictum*), Japanese larch (*Larix kaempferi*), and Sakhalin fir (*Abies sachalinensis*). Pastureland is sparsely distributed across the ARB. The population was approximately 76,000 and 62,000 as of 2010 and 2022, respectively (Ministry of Internal Affairs and Communications, 2022).

The various features within the ARB provide a challenging environment for streamflow estimation, which was one of the key reasons for choosing it as the study site in the present study. In addition, the streamflow of the Abashiri River has a local significance and socioeconomic impact on the fishery activities in Lake Abashiri. According to the official record, the annual commercial catch ($t \cdot year^{-1}$) and landing value (¥$\cdot year^{-1}$) recorded in Abashiri City had been increasing from the 1950s to 1980s, and have been reasonably stable at around 60,000 $t \cdot year^{-1}$ and 10 billion ¥$\cdot year^{-1}$ since then, respectively (https://www.city.abashiri.hokkaido.jp/030shisei/020toukei/080suisanntoukei/index.html). The annual commercial catch from the inland fishery in the Abashiri region was about 8% to 10% of its total catch (inland fishery and marine fishery) during the 1960s to 2000s, and 30% to 60% of which was contributed from the catch in Lake Abashiri. In terms of landing value, Lake Abashiri contributed more than half of the region's total inland fishery value. Shijimi (*Corbicula japonica*), Wakasagi (*Hypomesus nipponensis*), and Shirauo (*Salangichthys microdon*) are the three primary species for the fishery activities in Lake Abashiri. However, despite the present stable condition, a growing concern for the future river flow stability of the Abashiri River was expressed by the stakeholders of the Abashiri fishery community to the author in a previous interview. The socioeconomic significance of the local streamflow was another key reason for choosing the ARB as the study site in the present study. Landing value and commercial catch amount from the Ministry of Agriculture, Forestry and Fisheries of Japan (MAFF) statistics records (https://www.maff.go.jp/j/tokei/kouhyou/kensaku/bunya6.html) were used to evaluate the impact of future streamflow, discussed in section 5.2.

3. Boundary conditions for the future streamflow

3.1 Future climate

The future climate projection dataset used in this study was obtained from the JMA Regional Climate projection Data for Japan (previously named JMA Global Warming Projection Volume 9, JMA-GWP9), which was produced under the SOUSEI and TOUGOU programs. In the JMA-GWP9, the projections were made as of later decades of the 21st century (2076-2095) under two different future greenhouse gas concentration trajectories designed by the Intergovernmental Panel on Climate Change (IPCC), i.e., the Representative Concentration Pathway (RCP) 2.6 and 8.5. Prediction simulations yielded by a total of 28 coupled general circulation models from the Coupled Model Intercomparison Project Phase 5 (CMIP5) were initially derived under the two scenarios. Then, cluster analysis was performed on the prediction simulations regarding the sea surface temperature (SST) variations in the tropical regions, which significantly impact precipitation and atmospheric circulation. The clusters were classified into three patterns. Next, the three patterns and their averaged result were applied to future climate calculations via a global atmospheric general circulation model (AGCM) with a grid spacing of 20 km (Mizuta et al., 2012). Finally, a non-hydrostatic regional climate model (NHRCM) with a grid spacing of 5 km was used for the downscaling process to improve the calculations over extreme events, main mountain ranges, and main river basins in Japan (Sasaki et al., 2011). Averaged result of the four SST pattern-based climate calculations were used in this study as the future climate boundary conditions for the streamflow estimation. Specifically, daily precipitation (mm) and maximum and minimum temperature (°C) were used.

In addition, the dataset also includes a simulated climate of the present time (1980-1999), which was used in this study for comparison with the observation data from the Automated Meteorological Data Acquisition System (AMeDAS). The comparison was conducted for the bias correction to the obtained data, which was not initially conducted in the JMA-GWP9 as the bias systematic bias is expected to vary from region to region. Therefore, in this study, bias was corrected using the least square regression to the projection data of each month separately, assuming the systematic bias of JMA-GWP9 is consistent in all the grid points within the ARB, and between the present and future time.

Table 1. JMA-GWP9 projected climate change in the Abashiri region between the present (1980-1999) and the future (2076-2095). Present time and relative change values are from the averaged result of the four SST pattern-based climate calculations (N = 4). Value in brackets is the standard deviation in the 20 years of each period (N = 20).

Category	Present	RCP2.6	RCP8.5
Annual mean temperature (°C)	6.3	+1.7 (0.5)	+5.2 (0.7)
Days of max temperature > 30 °C (day)	8	+2.6 (3.2)	+17.0 (7.0)
Days of min temperature < 0 °C (day)	76	−21.5 (11.2)	−61.3 (8.1)
Times of hourly precipitation > 30 mm (n)	0	+0.1 (0.2)	+0.4 (0.5)
Annual max snow depth change (%)	100	−11 (21)	−45 (14)

By the end of this century, the global mean temperature is expected to rise by 2 °C and 4 °C in the RCP2.6 and RCP8.5, respectively. In the JMA-GWP9, the temperature change was projected to increase by 1.7 °C and 5.2 °C across the Abashiri region under the two scenarios, respectively. More specific changes are described in Table 1. The JMA-GWP9 and its previous versions have been frequently used in many climate change reports by the JMA, such as the Climate Change in Japan 2020 (https://www.data.jma.go.jp/cpdinfo/ccj/index.html). Therefore, the JMA-GWP9 was considered a suitable reference for setting this study's future climate boundary conditions. More details of the JMA-GWP9 are discussed in its official manual (https://www.data.jma.go.jp/cpdinfo/GWP/Vol9/pdf/gwp9_manual.pdf).

3.2 Future LULC

The future LULC projection dataset used in this study was developed based on the previous National Vegetation Surveys from the Ministry of the Environment of Japan, and a series of future assumptions for the possible future development direction in Japan up to 2050 (Saito et al., 2019; Shoyama, 2021; Shoyama et al., 2019). More specifically, assumptions were developed by the Predicting and Assessing Natural Capital and Ecosystem Services (PANCES) project, in which national-scale future scenario storylines for exploring potential changes in natural capital and ecosystem services until 2050 were designed (Saito et al., 2019). There are four PANCES scenarios: natural capital-based compact society (NC), natural capital-based dispersed society (ND), produced capital-based compact society (PC), and produced capital-based dispersed society (PD), in addition to the business-as-usual scenario (BaU). The scenarios were used as the theoretical basis for producing analyzable data in the geographic information system (GIS) platform (Shoyama, 2021; Shoyama et al., 2019). LULC maps at three different time points (1987, 1998, 2014) were initially derived based on the National Vegetation Surveys. Numerous vegetation categories were aggregated into 10 LULC classifications following the aggregation methods proposed by the National Institute for Environmental Studies (Akasaka et al., 2014; Ogawa et al., 2013). A change matrix was then

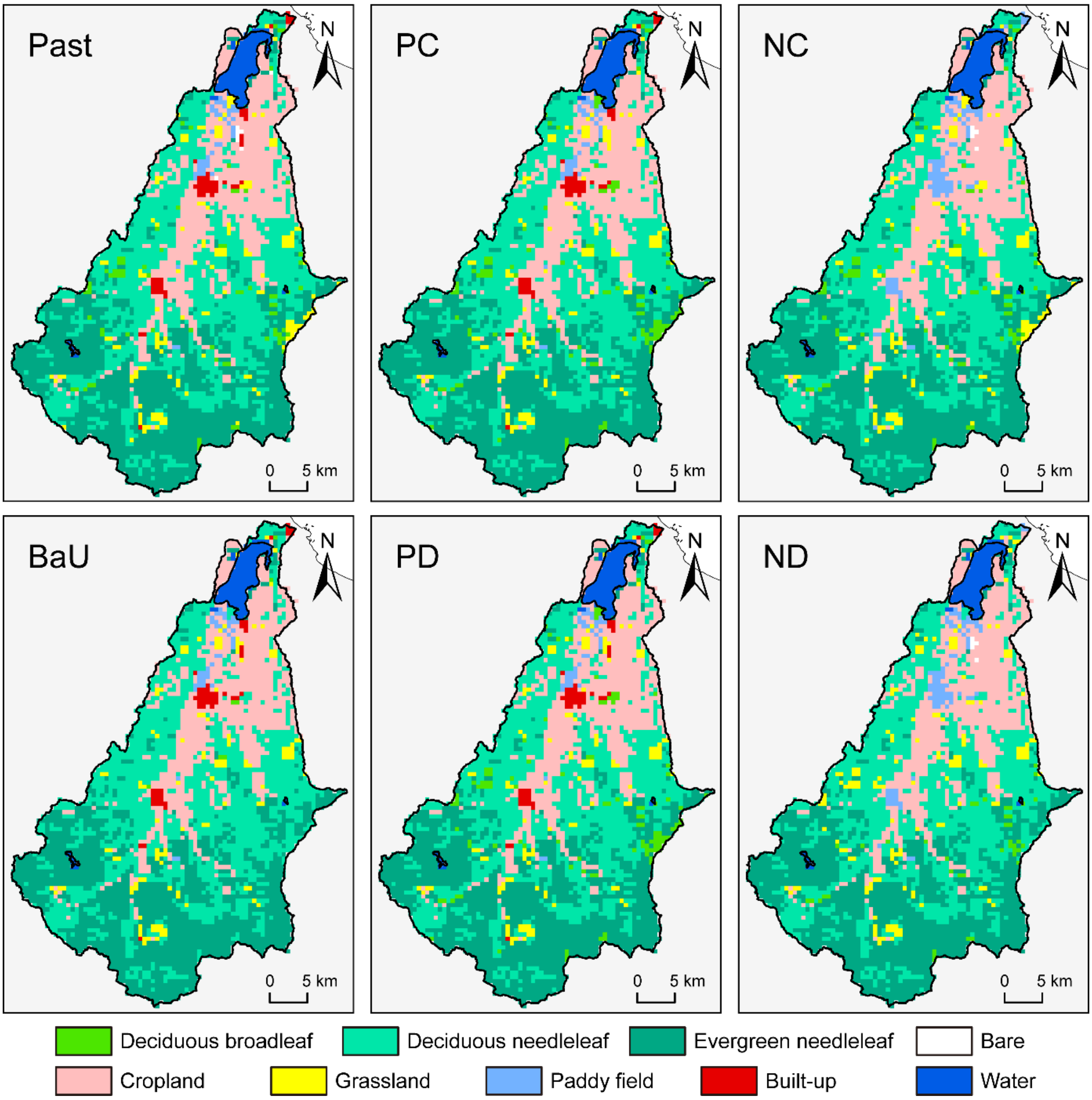

Fig. 2. LULC distribution in each scenario by the PANCES-LULC.

determined by analyzing the transitions between 1987 and 1998 using a multivariate function (Atkinson & Tatnall, 1997). The physical factors considered in the change matrix include elevation, slope, annual temperature, precipitation, distance to a stream, distance to a main paved road, and population density. A LULC simulation of 2014 was created using the change matrix and was then compared to the LULC map of 2014 as a validation of the matrix. After modifying the change matrix based on the comparison in 2014, a series of future development assumptions were integrated into the change matrix to simulate the future LULC GIS data (raster format) at a spatial resolution of 500 m. The LULC GIS data in the ARB was clipped from the original national-scale LULC dataset (hereinafter referred to as the *PANCES-LULC*) using ArcMap 10.7 software. The PANCES scenarios were determined via the participation of 15 research institutions and more than 100 researchers and policymakers in Japan. Therefore, this study considers the PANCES-LULC as a reasonable and conservative projection of the future. Even though the projected LULC in the ARB exhibits visually indistinct differences between the different scenarios (Fig. 2), significant relative change (Table 2) was found in classifications such as paddy field (+150% to +525%), built-up (−100% to +45%), and grassland (+45% to +50%). Relative change in forest coverage (5%) is quantitatively insignificant in comparison.

Table 2. LULC coverage (%) in each scenario by the PANCES-LULC.

LULC	Present	BaU	PC	PD	NC	ND
Water	2.6	2.6	2.6	2.6	2.6	2.6
Built-up	1.1	1.6	1.5	1.6	0.0	0.0
Paddy field	0.4	1.0	1.0	1.0	2.5	2.3
Cropland	21.3	20.2	20.2	20.2	20.3	20.3
Grassland	6.5	2.9	3.0	2.9	3.6	3.5
Deciduous broadleaf	2.9	0.2	2.6	2.6	1.7	0.9
Deciduous needleleaf	33.2	38.8	36.3	36.3	36.3	37.2
Evergreen needleleaf	32.0	32.8	32.8	32.8	32.8	32.8
Bare	0.2	0.0	0.0	0.0	0.1	0.1

4. Methodology

4.1 SWAT model

As introduced in chapter 1, hydrological distributed models are particularly suitable for future streamflow estimation as they can better consolidate the three crucial points on estimation reliability, i.e., physical complexity, partitioning on the sources of impact, and spatiotemporal scale. Therefore, SWAT (Arnold et al., 1998; Williams et al., 2008) was considered the appropriate tool for this study. SWAT is a basin-scale semi-distributed model capable of simulating streamflow quantity by tracking and calculating water transport through various components within the water cycle. As an open-access model, it is particularly suitable for studies under a data limitation, which is the primary setting in this study. SWAT has been widely used in numerous studies with various hydrological issues, including the streamflow estimation in response to climate and LULC changes (Abbaspour et al., 2015; Ficklin et al., 2009; Gassman et al., 2014; Wang et al., 2020). As SWAT was initially designed for managemental analysis on river basins, its reasonable physical complexity and the explicit partitioning on most of the water cycle components are particularly desirable for studies on this topic.

In SWAT, major model components include weather, hydrology, soil properties, plant growth, and land management (Fig. 3). SWAT divides the river basin into subbasins and then hydrologic response units (HRUs) for better representation of homogeneous land use property, topographical, and soil characteristics. Digital elevation model (DEM) data, LULC classification map, and soil property map are necessary as the model input to construct the HRUs.

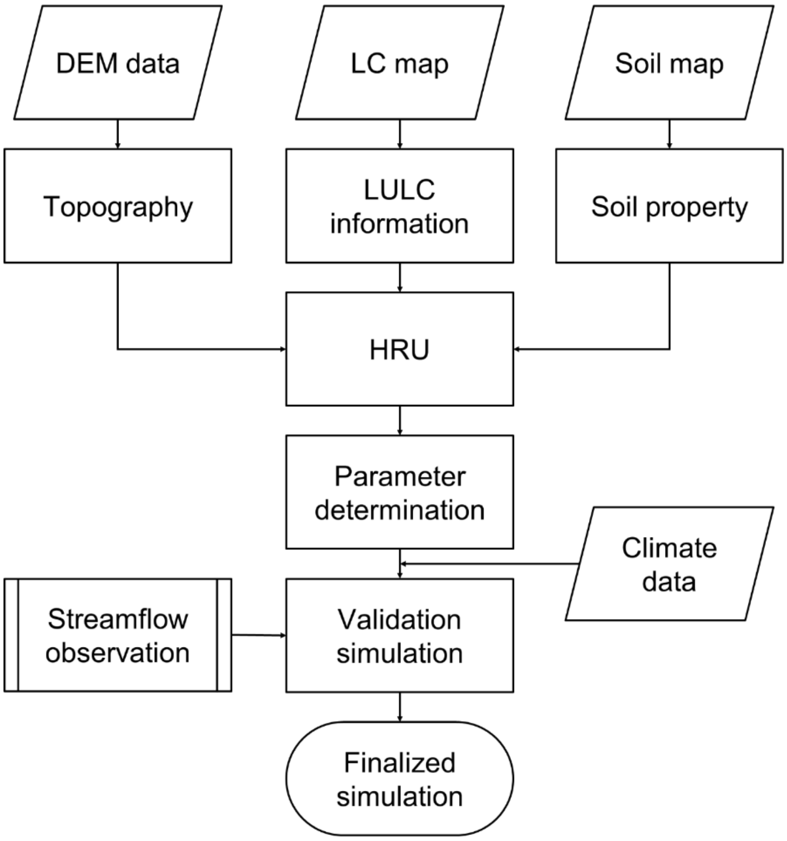

Fig. 3. Schematic of the basic structure of SWAT.

Daily calculations of water transport within the water cycle of each HRU follow the water balance as:

$$P = ET + Q + R + \Delta SW + \Delta GW \quad (1)$$

where P is precipitation (mm), ET is evapotranspiration (mm), Q is streamflow in the river channels (mm), R is surface runoff (mm), ΔSW and ΔGW are variation in the soil water storage (mm) and groundwater storage (mm), respectively. The water cycle is driven by climate, as it provides water content input and energy inputs. Accordingly, SWAT uses precipitation, maximum and minimum air temperature, solar radiation, relative humidity, and wind speed as the meteorological inputs. Simulation of catchment hydrology is separated into land phase and in-stream phase. Available water (mm) yielded from precipitated water, soil layers, and aquifers are first calculated in the land phase. Then, the streamflow ($m^3 \cdot s^{-1}$) is calculated in the in-stream phase. Anthropogenic factors such as artificial reservoirs and irrigation water use can also be specified if necessary. Due to the limited data availability, all the input data (Table 3) were obtained from open-access sources. Additional verification was conducted for each input to ensure its reliability.

Table 3. Description of input data used in SWAT model.

Data	Source	Resolution/scale
DEM	Digital Elevation Topographic Dataset, Geospatial Information Authority of Japan. (https://fgd.gsi.go.jp/download/ref_dem.html)	5 m and 10 m (grid)
LULC	ALOS High Resolution Land-Use and Land-Cover Map of Japan ver. 21.11, Japan Aerospace Exploration Agency. (https://www.eorc.jaxa.jp/ALOS/en/dataset/lulc_e.htm)	10 m
Soil	Comprehensive Soil Classification System of Japan First Approximation, National Institute for Agro-Environmental Sciences. (https://soil-inventory.rad.naro.go.jp/index.html)	1:200,000
Climate	Dynamical Regional Downscaling Using the JRA-55 Reanalysis (DSJRA-55), JMA. (http://jra.kishou.go.jp/DSJRA-55/index_en.html)	5 km (grid)

DEM is used to delineate the distribution of river channels and subbasin division, based on which the HRUs are defined and then used for calculations. First, basin delineation was performed using the Hydrology toolset in ArcMap ver. 10.7, then every delineated river channel and its corresponding subbasin boundary were verified (and manually modified when necessary) by the Geospatial Information Authority of Japan (GSI) at the finest zoom level available (1:2500). A total of 366 subbasins were identified, and used for calculations in this study.

LULC data is another critical inputs to delineate HRUs in SWAT. The ALOS LULC dataset was used in this study. ALOS LULC utilized numerous reference data during its initial production (e.g., Sentinel-2 Multispectral Instrument images, ALOS-2 Synthetic Aperture Radar images, ALOS PRISM Digital Surface Model dataset) in addition to the National Vegetation Surveys (the sole reference data for the former). Extensive verification was also conducted before the release (Hirayama et al., 2022), leading to a high resolution and considerably good spatial accuracy in the final product. Nevertheless, the classification within the ARB was verified in this study using both the GSI topographic map and satellite images from Google Earth Pro at the subbasin level. 12 types of classification were used in the original dataset, and nine were included within the ARB (Fig. 4a).

Soil type distribution data is the third critical input to delineate HRUs. In this study, it was not practically possible to directly verify the soil properties under limited data availability. Alternatively, the reported properties of each soil type were compared with that from the

FAO/UNESCO Soil Map of the World (http://www.fao.org/soils-portal/soil-survey/soil-maps-and-databases/faounesco-soil-map-of-the-world/en/). Eight different soil types by Great Group-division (21 by series group-division) were considered in this study (Fig. 4b). Based on the 366 subbasins, representative thresholds for the HRU determination (the percentage of a feature's coverage over the area of its subbasin) for slope, LULC, and soil type, were set as 15%, 10%, and 10%, respectively. 5055 HRUs were determined under this setting.

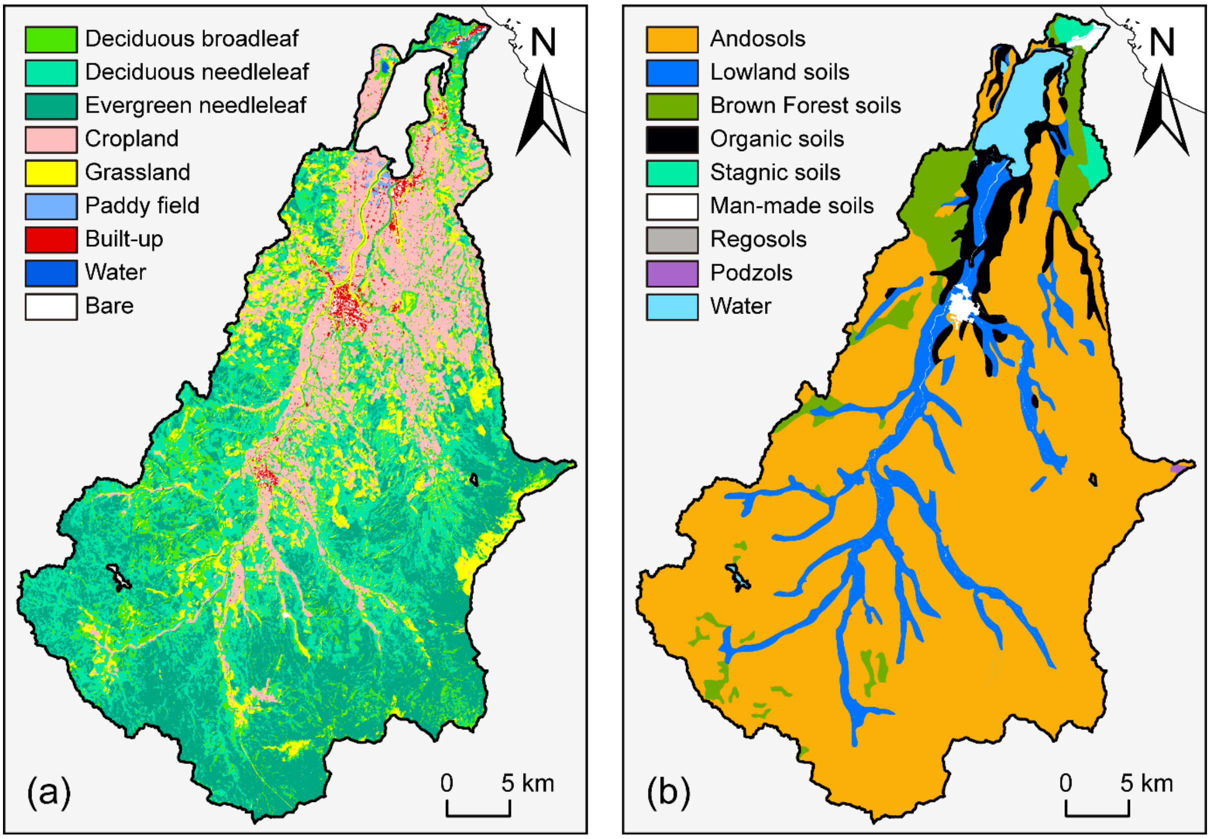

Fig. 4. LULC distribution map (a) and soil type distribution map (b) of the ARB, generated from the data listed in Table 3. For a clear illustration, only the eight Great Groups were included.

For the five types of meteorological input, SWAT requires hourly data for precipitation and daily data for the other four. The inputs were derived from the DSJRA-55 reanalysis data (Kayaba et al., 2016), of which 116 grid points were included in the ARB. Bias was evaluated and corrected before the release. It was concluded that a more considerable bias was observed in inland eastern Japan and the Pacific-side of northern Japan in the case of temperature, and in the Hokuriku region and Japan Sea-side of Honshu in the case of precipitation. On the other hand, the Abashiri region is among the areas where better agreements were found. In addition, it was mentioned that the reproductivity of extreme precipitation events over mountainous regions may require further improvement (Kayaba et al., 2016). However, as the reproductivity of extreme single-event was not the primary concern in this study, DSJRA-55 dataset was considered appropriate as the meteorological input. In the future streamflow simulations, ALOS LULC and DSJRA-55 were substituted by PANCES-LULC and JMA-GWP9, respectively. The former two datasets represent the present conditions for streamflow simulations, and the latter two represent the future conditions. The *t*-test was used to measure the difference between the present streamflow and future streamflow, in which a significant difference is described by a *p*-value that is lower than 0.05. Additionally, even though using different datasets between the present and future simulations may render the comparison between the two periods less rigorous, it was considered necessary to avoid more potentially significant uncertainty. More of this point is described in section 6.2.

4.2 Water cycle calculations and parameters

Most of the calculation processes in SWAT are performed at the unit of HRU (Fig. 5). Note that while SWAT provides multiple options for some of the processes (e.g., infiltration and potential evapotranspiration), this section only describes the ones used in this study.

Calculations of several major processes are described as follows.

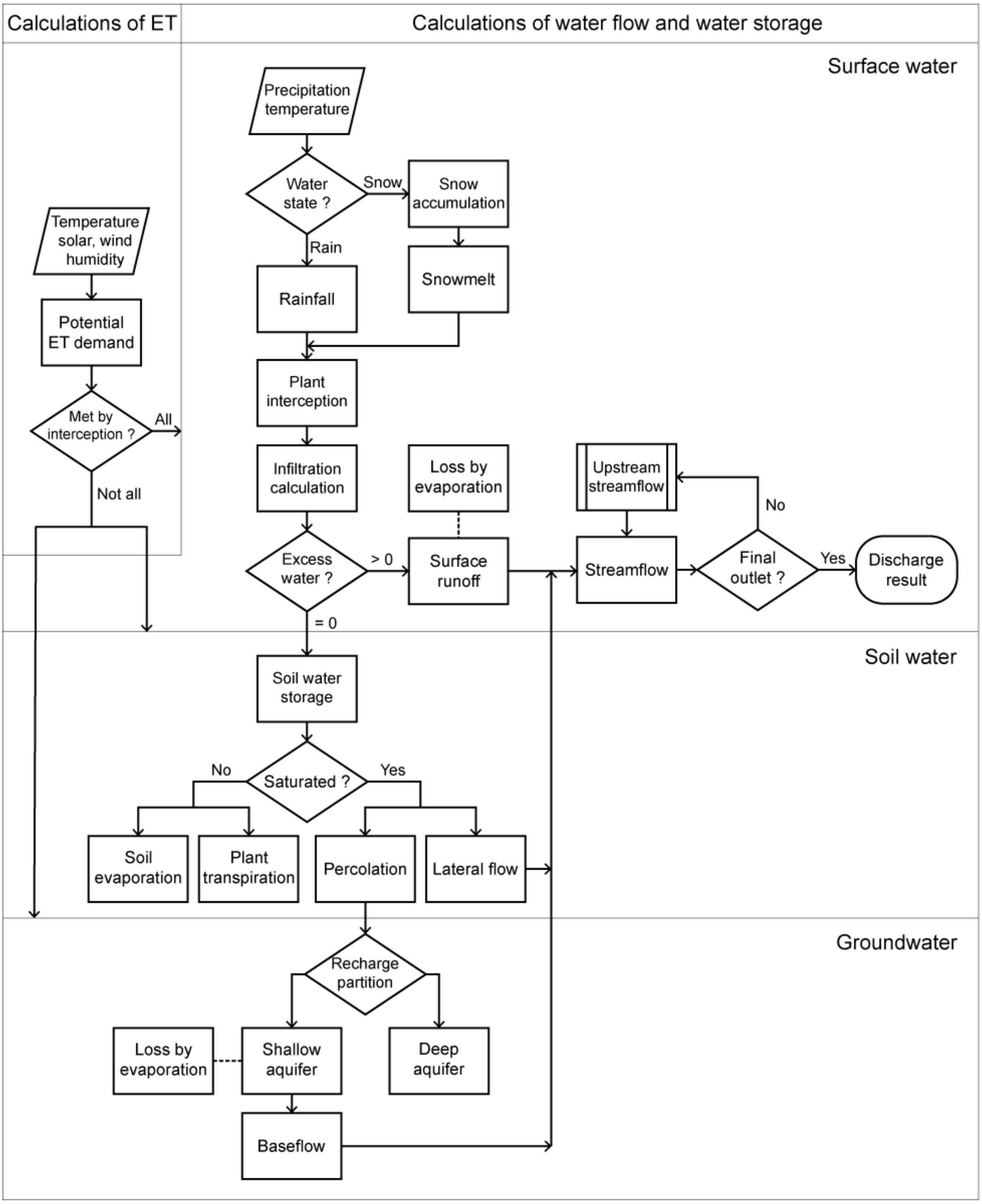

Fig. 5. Schematic of the water cycle calculation in a unit of HRU. Arrows indicate water movement through the water cycle; rhomboids are model input; rectangles are calculation processes; rhombuses are decisions; rectangles with double-struck edges are predefined processes; and the stadium is the calculation output.

1. Solar radiation. SWAT considers the radiant energy from the sun as the only energy source that impacts the earth's climatic processes. Net radiation (H_{net}, MJ·m^{-2}·d^{-1}) is described as:

$$H_{net} = (1 - \alpha) \cdot H_{SW} + H_{LW} \qquad (2)$$

where the arrows indicate the direction of the radiation flux, α is surface albedo, H_{SW} is incoming shortwave radiation (MJ·m^{-2}·d^{-1}), and H_{LW} is net (incoming – outgoing) longwave radiation (MJ·m^{-2}·d^{-1}). H_{SW} is from the solar radiation input, H_{LW} is determined by the Stefan-Boltzmann law of radiation:

$$H_{LW} = f_{cld} \cdot \varepsilon \cdot \sigma \cdot T_K^4 \qquad (3)$$

where f_{cld} is a factor to adjust for cloud cover described as a function of H_{SW} concerning the maximum possible solar radiation at the given latitude, ε is the net emittance between the atmospheric and vegetative emittance described as a function of vapor pressure on a given day (kPa) calculated from the relatively humidity input (Brunt, 1932; Jensen et al., 1990), σ is the Stefan-Boltzmann constant (4.903 × 10^{-9} MJ·m^{-2}·K^{-4}·d^{-1}), and T_K is the daily mean air temperature (K) calculated from the temperature inputs.

2. Potential evapotranspiration (PET). The daily heat flux is described using the Penman-Monteith method:

$$\lambda E = \frac{\Delta \cdot (H_{net} - G) + \rho_{air} \cdot c_p \cdot \delta e / r_a}{\Delta + \gamma \cdot (1 + r_c / r_a)} \tag{4}$$

where λ is the latent heat of vaporization (MJ·kg^{-1}), E is PET rate (mm·d^{-1}), Δ is the slope of saturation vapor pressure-temperature curve (kPa·°C^{-1}), H_{net} is the daily net radiation (MJ·m^{-2}·d^{-1}), G is ground heat flux (MJ·m^{-2}·d^{-1}), ρ_{air} is air density (kg·m^{-3}), c_p is the specific heat capacity of air (1.013×10^{-3} MJ·kg^{-1}·°C^{-1}), δe is vapor pressure deficit (kPa), γ is the psychrometric constant (kPa·°C^{-1}), r_a and r_c are the atmospheric resistance and canopy resistance (s·m^{-1}), respectively. More specifically, the value λ and Δ vary daily, as they are calculated from daily mean temperature; G is assumed as zero; δe is calculated from the temperature and relative humidity inputs; r_a is calculated as a function of inputted wind speed; r_c is calculated as a function of daily leaf area index, which varies according to the daily mean temperature; and γ is calculated as (Brunt, 1952):

$$\gamma = \frac{c_p \cdot p}{\lambda \cdot MW} \tag{5}$$

where p is atmospheric pressure (kPa) at a given elevation, MW is the ratio molecular weight of water vapor over dry air (0.622). The calculated PET is then used to calculate actual evaporation, transpiration and sublimation.

3. Snow accumulation and snowmelt. The mass balance of snow water content (*Snow*, mm) is described as:

$$\Delta Snow = P_{snow} - E_{sub} - Snow_{mlt} \qquad (6)$$

where P_{snow} is precipitation (mm) in the form of snowfall determined using the precipitation and temperature inputs, $Esub$ is daily sublimation (mm), and $Snow_{mlt}$ is the daily amount of snowmelt (mm). Daily snowmelt (mm·d^{-1}) is calculated using the degree day method (Anderson, 1976):

$$Snow_{mlt} = DDF \cdot (T - T_{mlt}) \qquad (7)$$

where DDF is the degree day factor on the day (mm·d^{-1}·°C^{-1}), T is the daily mean air temperature (°C), T_{mlt} is the threshold temperature (°C) above which snowmelt is allowed during the calculations.

4. Soil water. Infiltration of water through the ground surface is calculated using a modified Green-Ampt infiltration method (Mein & Larson, 1973):

$$f_t = K_e \cdot (1 + \frac{\Psi \cdot \Delta\theta}{F_t}) \qquad (8)$$

where f_t is the infiltration rate at time t (mm·hr^{-1}), K_e is the effective hydraulic conductivity (mm·hr^{-1}) calculated from the saturated hydraulic conductivity, Ψ is the wetting front soil suction head (mm) described as a function of porosity, percent sand and percent clay, $\Delta\theta$ is the change in water content across the wetting front (mm·mm^{-1}) described as a function of porosity and the available water capacity, and F_t is the cumulative depth of infiltration at time t (mm). Saturated hydraulic conductivity, porosity, percent sand, percent clay, and available water capacity are defined in the input of soil properties. This method assumes that the soil above the wetting front is entirely saturated, and the excess water on the ground surface is considered surface runoff. In addition to the Green-Ampt infiltration method, the Curve Number method (Mockus, 1972) is another option for infiltration calculations. It is more frequently used in SWAT applications as it requires daily precipitation data instead of subdaily. However, it has been pointed out that the Curve Number can lead to more significant model uncertainty, more likely than the Green-Ampt method, while its realistic determination requires in-situ measurements (King et al., 1999; Tasdighi et al., 2018). Given the limited data availability, this study considers the latter the preferable method. SWAT assumes the water distribution within the soil layer is uniform, meaning only the saturated flow is directly calculated, which includes lateral flow and vertical percolation. In contrast, unsaturated flow is indirectly modeled as two exponential functions that describe the distribution variations caused by soil evaporation and plant transpiration.

5. Groundwater. The saturated zone of groundwater is divided into an unconfined layer and a confined layer, i.e., a shallow aquifer and a deep aquifer. While the natural process of water transport in aquifers is from the shallow aquifer to the deep aquifer, SWAT applies a simple partition scheme that directly diverts the percolated water from soil layers. Therefore, water entering the deep aquifer within an HRU is excluded from later water budget calculations. The water in the shallow aquifer considers a water balance as:

$$aq_i = aq_{i-1} + w_{rchr} - w_{bf} - w_{loss} \qquad (9)$$

where aq_i and aq_{i-1} are the amount of water stored in the shallow aquifer (mm) on a given day and its previous day, w_{rchr} is the amount of recharge entering the shallow aquifer (mm), w_{bf} is the baseflow (groundwater contribution to the river channel; mm), and w_{loss} is the water loss through irrigation water use or a conditional evaporation process (mm).

6. Streamflow. Surface runoff, lateral flow from the soil layer, and baseflow from the shallow aquifer collectively become the available water for streamflow. As the in-stream phase of calculations, streamflow is calculated using the Muskingum routing method and Manning's equation. The Muskingum routing method uses a conservation of mass approach to route the flow. The total available streamflow water in a channel is conceptualized as the sum of prism and wedge storage:

$$V_{stored} = K \cdot (X \cdot q_{in} + (1 - X) \cdot q_{out}) \qquad (10)$$

where V_{stored} is water currently stored in the channel (m^3), K is the storage time constant for the channel (s), X is a weighing factor that defines the impacts between wedge and prism, q_{in} is the rate of inflow ($m^3 \cdot s^{-1}$), which includes both the outflow from the nearest adjacent up-stream HRU(s) and the generated water from the land phase of the current HRU, q_{out} is the outflow ($m^3 \cdot s^{-1}$) from the HRU, i.e., the streamflow, and functions as the q_{in} for the nearest adjacent downstream HRU.

In almost every calculation process described in this section, numerical parameters are involved either as threshold, coefficient, or definitional value in the corresponding equation. Therefore, appropriately determining the parameter values is essential to the model performance. Ideally, the parameters should be determined a priori, independently from the model's performance. However, in most distributed models, this becomes impossible due to their large number of parameters (Brutsaert, 2005). This study identified 35 parameters involved in the water cycle calculation. The alternative solution is statistical tuning, sometimes referred to as autocalibration, calibration, or optimization approach, and it has been considered conventional and inevitable in SWAT (Abbaspour, 2015; Abbaspour et al., 2015, 2018; Arnold, Moriasi, et al., 2012; Gassman et al., 2014). While minimizing the use of tuning in SWAT is not a necessarily unprecedented notion, a thorough discussion on its logical reasons and practical significance, especially under a representatively limited data availability, is yet to be appropriately presented. Therefore, this study proposes a consistent and physically meaningful manner to manually determine parameter values based on quantitative and qualitative empirical evidence. After the majority of parameters were determined, the remaining parameters left with relatively higher uncertainties were tuned using the SWAT Parameter Estimator of the SWAT Calibration and Uncertainty Procedures program (SWAT-CUP; Abbaspour, 2015) to improve the model performance. Model performance was measured by the Nash-Sutcliffe model efficiency coefficient (NSE; Nash & Sutcliffe, 1970), the Kling-Gupta efficiency (KGE; Gupta et al., 2009), and the coefficient of determination (r^2). The primarily determined and minorly tuned parameters was then used for model validation and for future streamflow simulations.

4.3 Minimizing the use of tuning

Tuning in hydrological models is an optimization process. While the tuning process has been developed from being more labor-intensive to more practically convenient and automated (Balascio et al., 1998), the model performance is always used as the benchmark. Therefore, this study argues that even when a satisfactory agreement between the simulation and observation was achieved by tuning, the physical meaning of the tuned parameters is not necessarily warranted to be reasonable to the local reality. Section 4.3 explains the logical reason and practical solution to this argument.

4.3.1 The conventional use of tuning

The model performance during tuning is measured by statistical quantities such as r^2, NSE, or KGE, generally referred to as the objectives of the tuning process. In other words, the only essential function of tuning is to optimize parameter values so that a satisfactory model performance may be reached. In contrast, the physical meaning of the tuned parameters is entirely neglected during the process, which is a potentially problematic issue because the physical meaningfulness and complexity are critical to the model's predictive power (Ludwig et al., 2009). However, the conventional argument considered in most previous studies is that if the sensitive parameters were tuned and led to satisfactory performance, the parameters must have been meaningful to a certain degree. As a result, most previous studies use a high-sensitivity result on the tuned parameters as the critical justification for the completion of tuning. In contrast to this conventional understanding, this study proposed a different argument. The parameter sensitivity is essentially the efficiency on the improvement of model performance, and is measured by statistical quantities. In the case of SWAT, tuning is commonly performed in SWAT-CUP, an interface developed primarily for tuning in SWAT, in addition to functions such as simulation validation and sensitivity analysis. In SWAT-CUP, the sensitivity of each parameter is measured by the *t*-test, where a high sensitivity is indicated by a higher absolute value of *t*-stat and a lower *p*-value (Abbaspour, 2015). Due to the large number of parameters, it is commonly considered impractical and logically unreasonable to tune all parameters simultaneously. As a result, less sensitive parameters would be excluded during tuning, leading to a small number of parameters for tuning. Owing to the tuning function, the unrealistic physical meaning of all the unadjusted parameters would be compensated by the fewer tuned ones, whose physical meaning was not warranted either. Moreover, as most of the water cycle processes and their corresponding calculations are directly or indirectly connected, the property of a given process can be altered by multiple parameters. Consequently, a cross-compensation effect may be generated, i.e., when tuning a certain number of parameters, the potential uncertainty of every parameter, either tuned or untuned, would all be distributed non-physically to the selectively tuned parameters and compensated. Ultimately, none of the parameters would necessarily become more physically meaningful, regardless of whether a satisfactory performance was achieved by tuning. As a result, the cross-compensation effect may lead to a matrix of incorrect representations of the natural processes that could collectively yield a conditionally satisfactory streamflow output.

Assuming the tuned parameters were significantly sensitive, the conditional performance of the physically unreasonable matrix could be acceptable for further simulations if a critical condition was met: the spatiotemporal settings between the tuned and further simulations were not significantly different. For example, the result of model validation in most previous SWAT applications follows this notion. However, the simulation of future streamflow does not comply with the critical condition. More specifically, the tuned parameters would be applied to the future in which the spatiotemporal setting (especially the temporal setting) is not necessarily comparable to that of the tuning simulation. For example, the parameters governed by the specific LULC type would be altered when the initial LULC input is replaced by its future version, thus violating the matrix. Therefore, minimizing the use of tuning is considered greatly important to the objective of this study.

4.3.2 The empirical approach

In response to the limited data availability, this study attempted to minimize the use of tuning in a consistent and physically meaningful manner by manually determining parameter values based on quantitative and qualitative empirical evidence (hereinafter referred to as the *empirical approach*):

1. The physical definition of every parameter involved in the water cycle and their interconnections were studied via an extensive search and reviews of existing literature (e.g., textbooks, physical manual of SWAT and functionally similar models, and journal papers).

2. The numerical value of each parameter was determined based on relative and comparable quantitative references.
3. Considering the paucity of direct measurement, qualitative references were used to compare the physical meaning of the determined value with the recorded local reality.
4. Questionable parameters were selected for further optimization by tuning based on the previous comparisons.
5. Considering the available computational power, parameters with significant physical impact on water quantity variation were used as the priority for tuning.

The following summarizes the considerations given for some of the parameters during the empirical approach. *Capitalized letters* are the parameter codes used in SWAT applications (Arnold et al., 2012).

SMFMX, SMFMN: maximum and minimum degree day factor value during a year ($mm \cdot d^{-1} \cdot °C^{-1}$). These two parameters governs the range of the *DDF* during the year in the Eq. 7 with a sinusoidal interpolation (Huber & Dickinson, 1988):

$$DDF = \frac{(SMFMX+SMFMN)}{2} + \frac{(SMFMX-SMFMN)}{2} \cdot \sin(\frac{2\pi}{365} \cdot (d_n - 81)) \quad (11)$$

where d_n is the Julian date of a year. By this interpolation, the seasonal variation of daily *DDF* values varies between the summer and winter solstices. The degree day method model has been validated as generally reliable in the case of Japan (Miyata et al., 2012). It has been reported that *DDF* may range from 1.4–6.9 in rural areas (Huber & Dickinson, 1988) to 0.9–7 in the case of Japan (Sakai, 1963). *DDF* during early April to early May in multiple locations on the western Hokkaido island has been estimated to vary from 3–4.5 (Hokkaido Electric Power Company & Sapporo Regional Headquarters of Japan Meteorological Agency, 1959; Sakai, 1963). Therefore, SMFMX and SMFMN were given as 5 and 1, respectively, to match the reported values at different times of the year.

CANMX, BLAI, T_BASE: maximum canopy storage capacity (mm), maximum leaf area index (LAI; $m^2 \cdot m^{-2}$), and minimum temperature for plant growth (°C). These three values differ on different LULC types. A portion of precipitation can be intercepted by plant canopy, which directly affects ET and varies between different types of vegetation and on different days:

$$can_{day} = CANMX \cdot \frac{LAI_{day}}{BLAI} \tag{12}$$

where can_{day} is daily canopy storage capacity (mm), LAI_{day} is daily LAI ($m^2 \cdot m^{-2}$) calculated as a function of temperature and regulated by T_BASE. As neither of the LULC datasets distinguishes forest by its species, the dominant forest species over the area of forest types in the ALOS LULC classification were first calculated according to the forest distribution record (Forestry Agency of Japan, 2013). The reported CANMX values from existing studies were then slightly modified accordingly (Attarod et al., 2014; Liu & Lobb, 2021; Nur Syahida & Azinoor Azida, 2018; Sato, 2014; Xiao & McPherson, 2016; Yu et al., 2012; Zou et al., 2015). A similar modification was given to T_BASE in the case of forest LULC types. For BLAI, the

MODIS 8-day LAI dataset was used (Myneni et al., 2015) to calculate the reasonable range of each LULC type in response to its maximum growth period. The properties of each plant and forest LULC type were found in multiple references (Hashizume et al., 1993; Horie, 2004; Karizumi, 2010; Miyabe & Kudo, 1986; Sato, 2014).

ESCO, EPCO: compensation factor (/) of soil evaporation and plant transpiration, respectively. The ability to meet the evaporative demand (PET) in the soil layers varies in different soil types and depths below the surface. An exponential function governs the variation related to depth, and the compensation factors can modify the significance of this function. No direct physical reference was found regarding the two parameters as they are specific to the SWAT applications. Nevertheless, ESCO was given to a difference between different soil types according to the permeability suggested in the input dataset of soil properties (https://soil-inventory.rad.naro.go.jp/index.html).

ALPHA_BF: inverse of the baseflow recession constant. SWAT considers baseflow recession as an exponential decay process:

$$Q_{bf} = Q_{bf,0} \cdot \exp(-t \cdot ALPHA\_BF) \qquad (13)$$

where Q_{bf} is baseflow contribution rate ($m^3 \cdot s^{-1}$), $Q_{bf,0}$ is baseflow rate at the beginning of period, t is time (s). The inverse of ALPHA_BF, i.e., the baseflow recession constant (day), is the function of hydraulic conductivity, specific yield, and average flow distance of the shallow aquifer (Brutsaert, 2005). While this parameter usually exhibits lower sensitivity during tuning due to its function, it is one of the vital characteristic parameters of groundwater contribution. Observed daily streamflow data over three stations were used to calculate ALPHA_BF using six different methods (Kroll, 1989; Vogel & Kroll, 1996). A value of 0.97 is given to the basin, indicating a rapid response to groundwater release (Neitsch et al., 2011).

GW_REVAP: compensation factor (/) for shallow aquifer evaporation. The effect of this parameter is the same as EPCO and ESCO, as to adjust the evaporative demand. However, the evaporation process here refers explicitly to where water is removed from the shallow aquifer through the vadose zone to the surface and evaporates. This parameter is specific to the use of SWAT applications. Its value was suggested to be 0.02-0.20 with no physical explanation (Arnold et al., 2012). Liu et al. (2004) detailed this parameter in an arid region and reported a range of 0.05–0.30. Additionally, their study did not involve any use of SWAT and concluded that the parameter varies depending on the land cover and groundwater depth, and should generally be considered less significant in less arid regions than the study area they used (inner Mongolia). Therefore, a value of 0.02 was given.

OV_N, CH_N: the Manning's roughness coefficient (n) in surface runoff and river channel flow, respectively. The determination of n generally requires field measurement, such as inflow and outflow during a specific section of the channel, as well as its geometry information. In the absence of observation, n can be approximated based on the characteristics of the channel, such as slope, vegetation, and level of meandering (Arcement & Schneider, 1989). By crosscomparing multiple reported variations of n, values ranging from 0.01-0.2 were given to OV_N for different LULC types (Arcement & Schneider, 1989; Downer & Ogden, 2006; Engman, 1986), and a value of 0.05 for river channel flow (Arcement & Schneider, 1989; Chow et al., 1988; Hornberger et al., 2014; Japan Society of Civil Engineers, 2019).

Information on the remaining parameters is summarized in Table 4. Most of the 35 parameters were determined by direct calculation, or based on quantitative results reported in other comparable locations or qualitative results reported in the ARB. In the fourth step of the empirical approach, nine parameters were selected (bold ones in Table 4): SFTMP (snowfall threshold temperature, °C), SMTMP (snowmelt threshold temperature, °C), SNOCOVMX (minimum snow water content at 100% snow coverage, mm), SNO50COV (snow water content at 50% snow coverage over SNOCOVMX, %), SOL_AWC (soil water capacity, %), GW_DELAY (constant of groundwater delay, day), MSK_X (weighting factor X in Eq. 10), MSK_CO1, 2 (tuning factors in the Muskingum equation). Finally, the following four parameters were considered the priority to be tuned.

SFTMP, SMTMP: threshold temperature (°C) for snowfall and snowmelt process. Both parameters were initially set as zero following their most general definition. However, coarse partitioning of the precipitation phase in modeling works may lead to significant biases in snow-related calculations, which propagates into errors in streamflow (Gascón et al., 2018; Jennings et al., 2018). Consequently, even a slight change in their values could lead to a significant difference in water content in the water cycle. Therefore the parameters were included in the tuning process, after which SFTMP was adjusted to 3.2, and SMTMP was adjusted to 1.9.

GW_DELAY: constant of the delay effect in groundwater recharge (day). This parameter is involved in an exponential decay function, similar to ALPHA_BF and SURLAG. The function is used here to represent the time delay from water passing through the soil profile via percolation to the point where it enters the shallow aquifer as recharge. In reality, this period depends on the depth of the groundwater table, and the hydraulic properties of the geologic formations in both the vadose zone (unsaturated zone) and the groundwater zone (saturated zone). The current data availability could not match the physical complexity of this parameter. Therefore it was considered necessary to be included in the tuning process. GW_DELAY was adjusted to 327.

SOL_AWC: available water capacity (/). Available water is the difference in water contents at field capacity and wilting point. It is defined as the amount of water available for uptake by plant roots. This concept is frequently used in agronomic engineering and modeling (Cassel & Nielsen, 1986). This parameter significantly affects the availability of soil moisture, which controls the rates of evaporation and transpiration, and indirectly affects infiltration and groundwater recharge (Hong et al., 2013). Due to its physical importance and the lack of measurements, it was considered necessary to include SOL_AWC in the tuning process. In addition, the value of SOL_AWC varied on different soil types and was included in a pre-defined database of SWAT. The tuning process applied a relative change to the pre-defined values so that the heterogeneity could be maintained. The pre-defined values ranged between 0.10-0.18 and were adjusted to 0.40-0.71 after the tuning (× 3.8). All parameters in the *t*-test showed acceptably high absolute *t*-stat values and significant *p*-values ($p < 0.01$). The significance of the empirical approach is discussed in section 6.1.

Table 4. Numerical value of all the identified parameters in water cycle calculations. *Name* is the parameter code name in SWAT, excluding *Albedo*, which refers to the plant albedo in Eq. 1:1.2.15 in the official SWAT manual (Neitsch et al., 2011). *Default* refers to the default value initially given in SWAT. The default value was left intentionally unchanged for several parameters according to the found references, otherwise marked as bold. Value range indicates an HRU-level parameter with one value on each LULC, soil, or slope class, not the meaning of a varying value during the calculations.

Name	Definition (unit)	Default	Determined
SFTMP	Snowfall threshold temperature (°C).	1	0
SMTMP	Snowfall threshold temperature (°C).	0.5	0
SMFMX	Maximum degree day factor ($mm \cdot d^{-1} \cdot °C^{-1}$).	4.5	5
SMFMN	Minimum degree day factor ($mm \cdot d^{-1} \cdot °C^{-1}$).	4.5	1
TIMP	Temperature lag factor of snowpack.	1	0.75
SNOCOVMX	Minimum SWE at 100% snow coverage (mm).	1	90
SNO50COV	SWE at 50% snow coverage over SNOCOVMX (/).	0.5	0.5
CANMX	Canopy storage capacity (mm).	0	[0, 2.5]
ESCO	Soil evaporation compensation factor.	0.95	[0.8, 1]
EPCO	Plant transpiration uptake compensation factor.	1	[0.1, 1]
RCHRG_DP	Deep aquifer percolation fraction (/).	0.05	0.04
GWQMN	Threshold water level of baseflow occurrence (mm).	1000	[700, 780]
ALPHA_BF	Inverse of the baseflow recession constant (day^{-1}).	0.048	0.97
GW_DELAY	Aquifer recharge delay time (day).	31	31
GW_REVAP	Compensation factor of aquifer evaporation.	0.02	0.02
REVAPMN	Threshold water level of aquifer evaporation (mm).	750	1000
SURLAG	Lag coefficient for surface runoff.	4	5
CH_N(1)	Manning's *n* for river flow in tributary channel.	0.014	0.05
CH_K(1)	Hydraulic conductivity in tributary channel (mm/h).	0	0
CH_N(2)	Manning's *n* for river flow in main channel.	0.014	0.05
CH_K(2)	Hydraulic conductivity in main channel (mm/h).	0	0.03
EVRCH	Coefficient for river evaporation loss adjustment.	1	1
EVRSV	Coefficient for lake evaporation loss adjustment.	0.6	0.75
MSK_X	Weighting factor in Eq. 10.	0.2	0.2
MSK_CO1	Impact factor of normal flow in Muskingum method.	0.75	0.75
MSK_CO2	Impact factor of low flow in Muskingum method.	0.25	0.25
OV_N	Manning's *n* for overland flow.	[0.01, 0.15]	[0.01, 0.2]
BLAI	Maximum leaf area index of plant ($m^2 \cdot m^{-2}$).	[0, 5]	[0, 7.5]
ALAI_MIN	Minimum leaf area index of forest ($m^2 \cdot m^{-2}$).	0.75	[0.05, 0.5]
T_BASE	Base temperature for plant growth (°C).	[0, 12]	[0, 8]
SOL_AWC	Available water capacity of soil (/).	[0.1, 0.18]	[0.4, 0.74]
CHTMX	Maximum canopy height (m).	[0, 10]	[0, 30]
RDMX	Maximum root depth (m).	[0, 3.5]	[0, 3]
CO2	Carbon dioxide concertation (ppmv).	330	380
Albedo	Representative plant albedo at minimal snow cover.	0.23	0.1

4.4 Additional data and modifications

The presentation of water bodies such as lakes and dams can be specified in SWAT as additional input. Three water bodies in the ARB with considerable surface areas were included in this study: Lake Abashiri, Lake Chimikeppu, and Furuume Dam. SWAT provides the option to simulate the water outflow from the water body, or to specify the outflow according to observation data. Primary inputs include surface area and water volume at normal and emergency conditions. An annual mean outflow rate or monthly mean outflow rate at each month is needed in the case of simulated outflow. The outflow from Lake Chimikeppu was simulated, and the required inputs were defined according to the 4th Natural Environment Survey on Inland Waters (1991). The outflow from Furuume Dam was simulated based on the official information (Table 5). For Lake Abashiri, observed daily streamflow data at the Omagari Station (Fig. 1) was used to specify the outflow directly.

Table 5. Information of Furuume Dam presented at the dam station (43°41′50″N 144°13′33″E).

Definition (unit)	Value	Definition (unit)	Value
Catchment area (km^2)	15.00	Effective water depth (m)	23.50
Reservoir area (km^2)	0.29	Design flood ($m^3 \cdot s^{-1}$)	200.00
Reservoir capacity (hm^3)	3.50	Maximum withdrawal ($m^3 \cdot s^{-1}$)	1.49
Active storage capacity (hm^3)	3.23	Maximum release ($m^3 \cdot s^{-1}$)	7.04

SWAT provides several fairly straightforward options for representing irrigation water use over paddy fields. Previous studies have pointed out the limitations of these options and developed separate modules as a substitute for more robust simulations (e.g., Kang et al., 2006;

Sakaguchi et al., 2014; Tsuchiya et al., 2018). However, paddy field coverage in such studies (9% to 19%) is much more significant than in this study (0.3%). Furthermore, the additional modules commonly require more specific data, such as observed flow rate at irrigation canals or water depth measurement in the paddy field, which were not available in this study. Considering the research purpose and data availability, irrigation water use for the paddy field was estimated following the principles described by Nakagawa (1966). Paddy field irrigation water use is distinctively different over two stages, the puddling stage and the regular stage. Water balance (mm) during the puddling stage can be described as:

$$w_{pud} = w_{inu} + air_A + air_B + E + p \qquad (14)$$

where w_{pud} is net water requirement during puddling stage, w_{inu} is inundation amount, E is evaporation over field surface, p is outward percolation amount, air_A and air_B are exchanged air amount in soil horizon A (Sakudo) and B (Shindo), respectively. Eq. 14 incorporates exchanged air amount puddling stage is essentially a process where the unsaturated soil gets inundated to reach complete and steady saturation (Nakagawa, 1966). Water balance (mm) during the regular stage can be described as:

$$w_{re} = E + p + w_{lot} - P_{effc} \qquad (15)$$

where w_{re} is net water requirement during regular stage, w_{lot} is water requirement for lot-management, P_{effc} is effective rainfall. Lot-management refers to the process after the midsummer drainage where constant ponding needs to be maintained. The gross water requirement during both stages equals the sum of net water requirement, conveyance loss, and management water requirement. Considering the data limitation, Eqs. 14 and 15 were simplified according to the empirical records concerning the cultivation pattern of rice (Horie, 2004; Maruyama, 1986; Nakagawa, 1966). w_{pud} was assumed to be 120 mm -180 mm for a well-drained field during the puddling stage. E was consider proportional (0.93) to PET (Odani, 2015), and PET is the SWAT-calculated value in the subbasin at which the field is located. $p + w_{lot}$ was substituted by the standard optimum percolation level (15 mm·d^{-1} - 25 mm·d^{-1}). P_{effc} was considered zero as daily mean was smaller than 5 mm. The sum of conveyance loss and management water requirement was considered 20% of w_{re}. The paddy field area was derived from the ALOS LULC dataset and verified with data from the MAFF statistics database (https://www.maff.go.jp/j/tokei/kouhyou/sakumotu/menseki/index.html).

5. Streamflow of the ARB

5.1 Finalized simulation

After applying the empirical approach, the daily observation data during 2001-2005 (Fig. 6) was used as the benchmark for tuning the parameters to improve the model performance. Parameter values were then maintained to produce the daily simulation in 2006-2010 as the validation (Table 6). Preferable value ranges of NSE, KGE, and r^2 are > 0.5 (Ritter & Muñoz-Carpena, 2013), > 0 (Knoben et al., 2019), and > 0.5, respectively. A general agreement between the simulation and observation was reasonably satisfactory across the ARB. Daily simulations during 2001-2010 were then used as the present level for comparisons with future simulations. It should be noted that ideally, the period considered in tuning should match with that in the future meteorological data (2076-2095). However, a 20-year tuning was not considered impractical, considering the available computational power in this study. Alternatively, the 5-year tuning was conducted, and a 10-year period (2001-2010) was used as the present benchmark. In the case of streamflow under the future LULC condition, the 5-year period (2001-2005) was used as the benchmark, because the LULC projection was initially made with a 5-year interval. In addition, it is considered necessary and meaningful to use the simulated results (instead of the observation) for comparisons, as the changing drivers that affect the streamflow could be explicitly controlled in this manner.

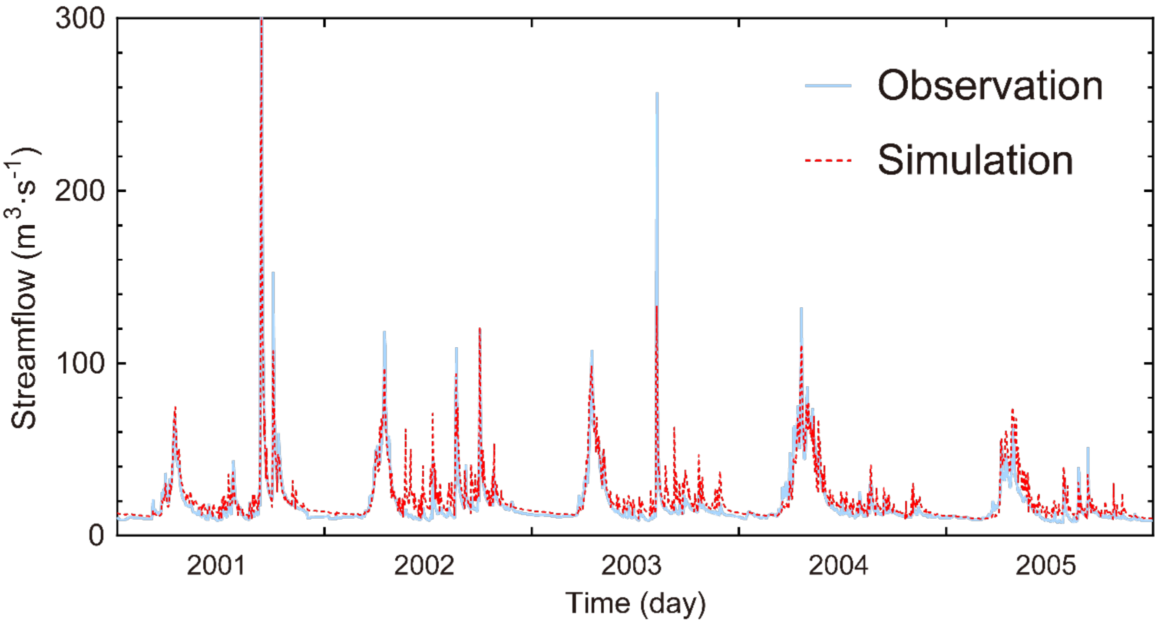

Fig. 6. Comparison between the observation and the finalized simulation at Hongou station.

In addition to the overall satisfactory model performance, higher discrepancies were found during summer and extreme events. The overestimation of streamflow during summer was most likely due to the underestimation of ET, which could be resulted from the limitation of plant growth representation in SWAT, and has been frequently noted in previous studies (e.g., Strauch & Volk, 2013; Zhang et al., 2020). Possible solutions could be an extensive modification to the initial Heat Unit database of SWAT, or an individually developed module, both of which, however, require the in-situ observation of plant growth. Moreover, while tuning the parameters directly involved in the ET (e.g., ESCO, EPCO, GW_REVAP) may lead to a less significant underestimate, such an attempt was not conducted in this study to avoid excessive tuning. On the other hand, the underestimation of streamflow during extreme events was most likely caused by another systematic limitation of SWAT. It was particularly noted in the official manual of SWAT that the model is a continuous time model and was not designed for robust simulation of single-event flooding. Therefore, the tuning process was not able to significantly remedy the discrepancy. Nevertheless, the simulation appropriately reproduced each actual extreme event, and the finalized model was considered adequate for producing future streamflow simulations. Furthermore, most of the results in sections 5.2 and 5.3 were derived from the same subbasin in which Hongou station is located, from which the outflow directly contributes to Lake Abashiri.

Table 6. Evaluation of the finalized simulations. The lower-stream and upper-stream locations refer to Hongou (1,120 km^2) and Tsubetsu stations (571 km^2), respectively (Fig. 1).

Location	Tuning (2001-2005)			Validation (2006-2010)			Validation (1991-1995)		
	NSE	KGE	r^2	NSE	KGE	r^2	NSE	KGE	r^2
Lower-stream	0.77	0.71	0.81	0.67	0.69	0.68	0.49	0.63	0.55
Upper-stream	0.75	0.73	0.77	0.68	0.70	0.70	0.50	0.66	0.58

5.2 Streamflow under future climate conditions

Averaged streamflow results were compared between the present time (2001-2010) and the two future scenarios (RCP2.6, RCP8.5; 2076-2095). This section describes the climate-induced streamflow change (ΔQ_{clim}), marked by number for the convenience of reference in their corresponding interpretations, in which possible reason, implication, or both are discussed. Additionally, the *significance* of change is indicated based on the *p*-value in the *t*-test, where a significant difference is noted when $p < 0.05$, and vice versa. Daily streamflow (Fig. 7a) at present begins to increase in late March and reaches its peak in mid-April. After that, the streamflow decreases until early July and varies fairly frequently in autumn. Secondary peaks occur in September and October, then the streamflow decrease in November until the baseflow level is reached and maintained during the winter. Compared to the present level, significant changes in the RCP2.6 scenario include (1) a decrease in late March (March 16-29); and (2) an increase in late August (August 22-29). Significant changes in the RCP8.5 scenario include (3) a decrease in mid-March (March 6-19); (4) a decrease in early April (April 2-8), in addition to (5) a two-week early shift of the peak flow occurrence; and (6) a decrease from late April to June (April 19-July 2). Streamflow between the two scenarios showed (7) a significant difference in early April (March 31-April 4). In the case of monthly streamflow (Fig. 7b), significant decreases were found in (8) March in the RCP2.6 scenario, and in (9) May and June in the RCP8.5 scenario. Additionally, no significant difference was found in the monthly streamflow between the two scenarios. In the case of flow regime (Fig. 8), no significant change was found in the RCP2.6 scenario, whereas the (10) low flow, droughty flow, and average flow showed a significant decrease in the RCP8.5 scenario. Moreover, a significant difference between the two scenarios was found in the high flow.

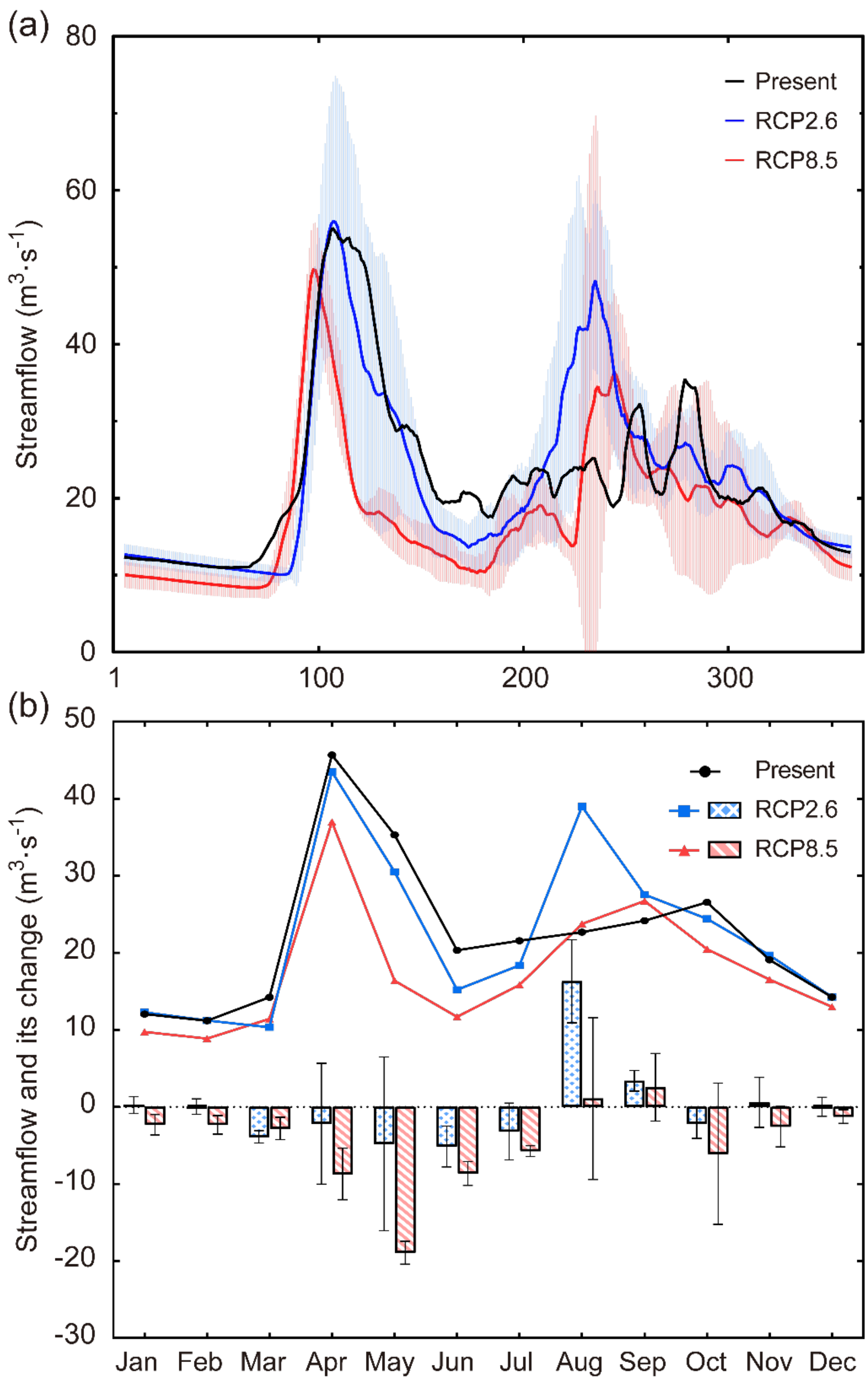

Fig. 7. (a) 10-day averaged daily streamflow in the present and the two future climate scenarios. The horizontal axis is the day of the year. The shades are the standard deviation of the future streamflow, generated from the multi-year climate projection input. (b) Monthly streamflow in the present and the two future climate scenarios. Column and error bar are the absolute change and standard deviation of streamflow in each month, respectively.

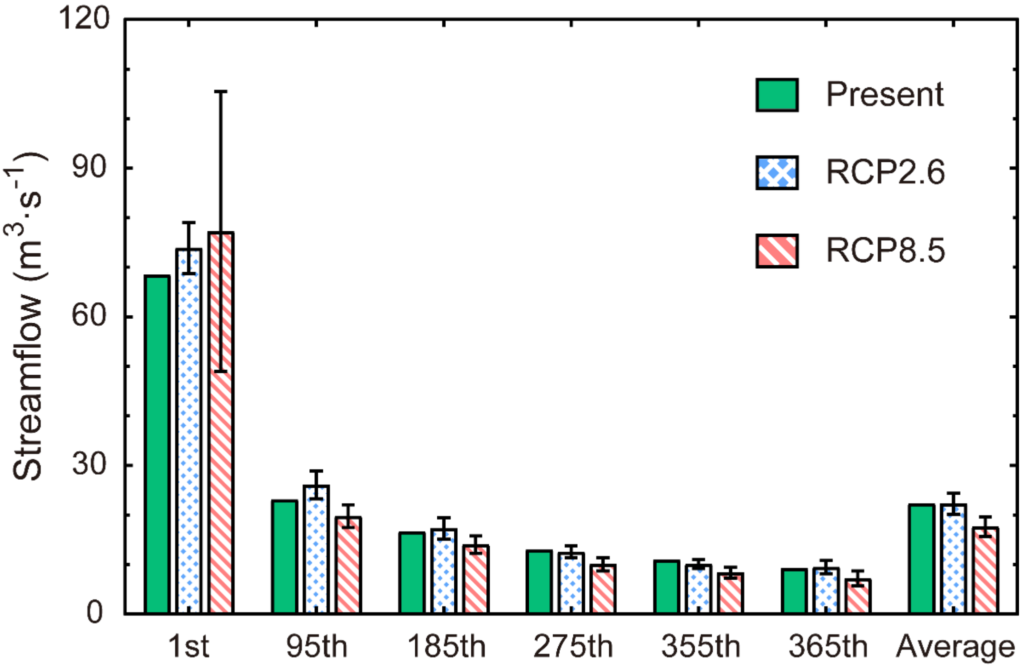

Fig. 8. Averaged flow regime in the present and the two future climate scenarios. Flow regime index (except the average flow) is derived by arranging the daily streamflow of a year in descending order, where the 1st, 95th, 185th, 275th, 355th, and 365th quantity is referred to as the maximum flow, high flow, median flow, low flow, droughty flow, and minimum flow, respectively. The error bar is the standard deviation of each index, generated from the multi-year climate projection input.

Between the present and future streamflow results, the climate conditions (Fig. 9) were the only source of difference. ΔQ_{clim} (1) and ΔQ_{clim} (3) are likely related to the change in monthly mean temperature in March. Compared to the present level, the timing when the temperature becomes positive is approximately a month earlier in the RCP8.5 scenario, which also explains the early shift in ΔQ_{clim} (5). The significant decrease in winter precipitation also significantly impacted the streamflow during the melting season by causing a significant decrease in snowmelt in both scenarios (Fig. 10). However, the change of snowmelt behaves differently between the RCP2.6 and RCP8.5 scenarios. In the former case, the impact is mainly from the decrease in winter precipitation, which resulted in a significant decrease in snowmelt in March, which explains ΔQ_{clim} (8). In the latter case, the timing change in temperature and the decrease in winter precipitation collectively led to a significant change in timing and quantity in snowmelt. The difference between the two scenarios is the possible reason for ΔQ_{clim} (4, 7), whereas the more significant decrease of snowmelt in the RCP8.5 scenario most likely led to the decrease of streamflow in May in ΔQ_{clim} (6, 9). On the other hand, the significant decrease of streamflow in June in the RCP8.5 in ΔQ_{clim} (6, 9) is most likely caused by the significant increase of temperature in summer via the increase of actual ET (Fig. 11). The different change in ET between the two scenarios led to some noticeable differences in the streamflow. For example, in autumn, the highly variable precipitation led to the increase in ΔQ_{clim} (2) in the RCP2.6 scenario. In contrast, the more significantly increased ET in the RCP8.5 scenario suppressed the impact of precipitation and led to the insignificant quantity change in streamflow. Another example of the different change in ET can be found during winter, which is more visually noticeable in its spatial distribution than in Fig. 11. In Fig. 12, a distinct difference in winter streamflow change was simulated, despite the similar change in precipitation. This difference may be explained by the difference in ET, which received impacts from precipitation and temperature differently between the two scenarios. More specifically, in the RCP2.6 scenario, the impact of the decreased precipitation had a more dominant impact than the temperature on the change of ET, which likely caused a decrease in water content available for evaporation. As a result, despite the increase in temperature (therefore, the increase of PET), winter ET decreased in the RCP2.6 scenario. In contrast, in the RCP8.5 scenario, the increased temperature had a more dominant impact than precipitation on the change of ET. As a result, winter ET increased in the lower-stream area of the ARB in the RCP8.5 scenario.

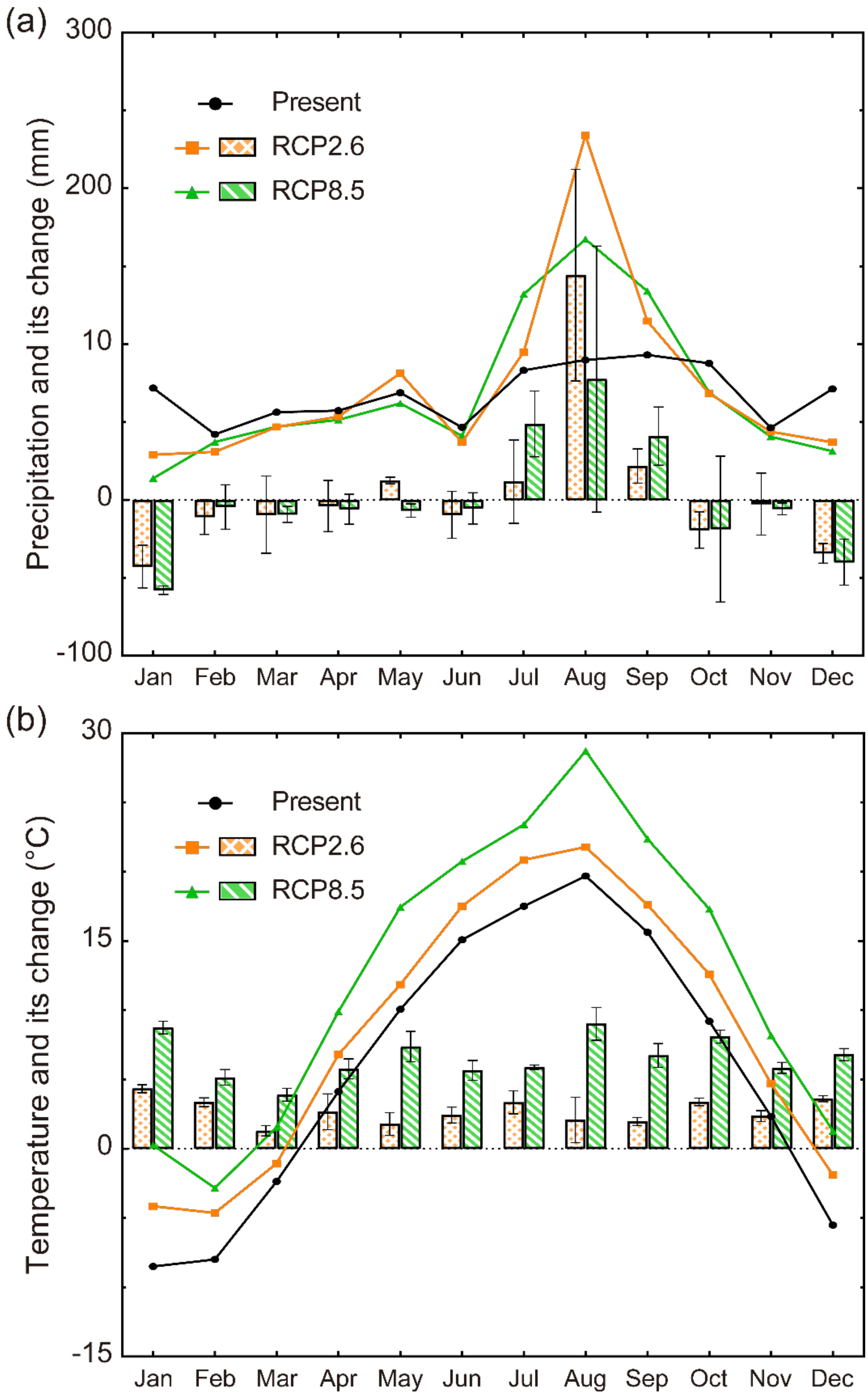

Fig. 9. (a) JMA-GWP9 projected monthly mean precipitation in the present and the two future climate scenarios. Columns and error bars are the absolute change and standard deviation of precipitation in each month, respectively. In both scenarios, the decreases in January and December are significant. The increase in July in the RCP8.5 scenario is significant as well. The difference in May is significant between the two scenarios. (b) Same as in Fig. 9a but for monthly mean temperature. Compared to the present level, the increases in all months are significant, except in August in the RCP2.6 scenario. The difference between the two scenarios is significant every month. Note that these are not strictly the *results* of the present study, but were allocated here for the convenience of reference.

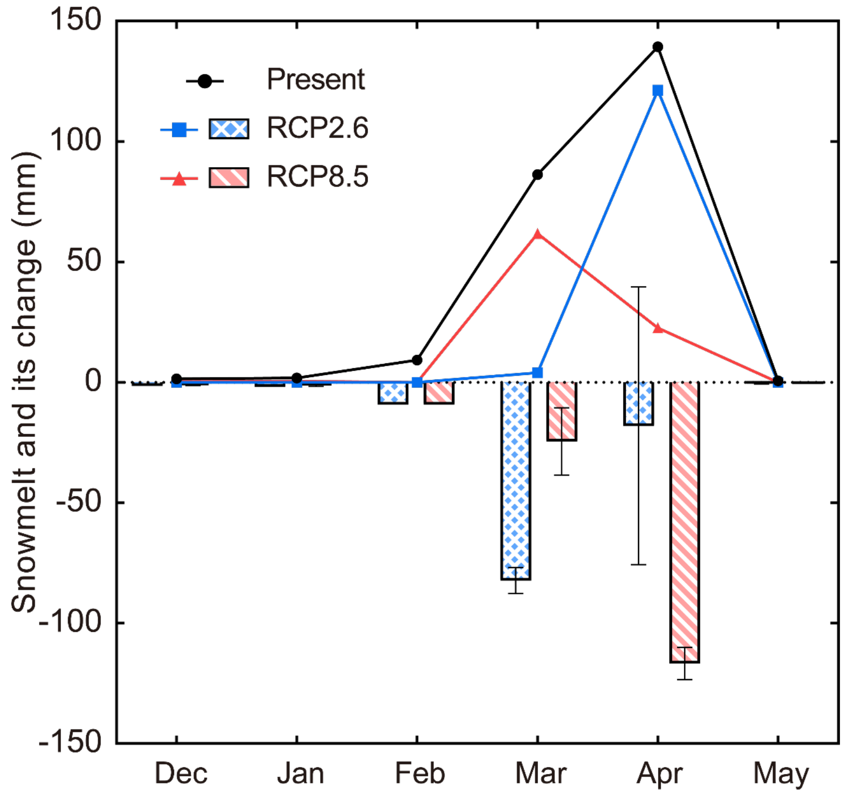

Fig. 10. Monthly snowmelt in winter-spring in the present and the two future climate scenarios. Column and error bar are the absolute change and standard deviation of snowmelt in each month, respectively.

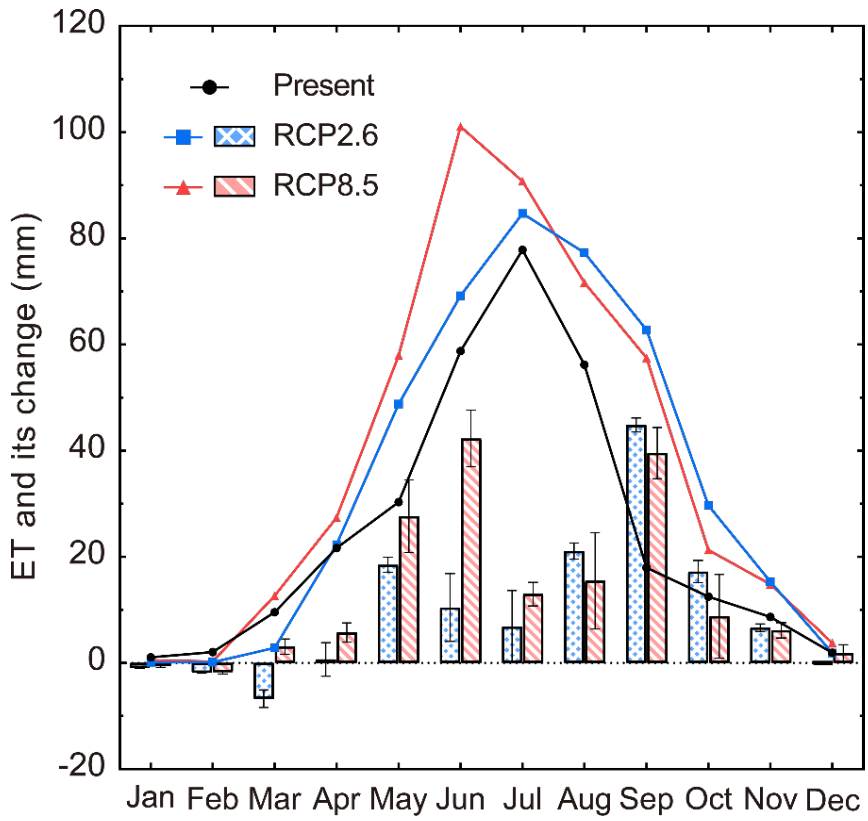

Fig. 11. Monthly ET in the present and the two future climate scenarios. Column and error bar are the absolute change and standard deviation of ET in each month, respectively.

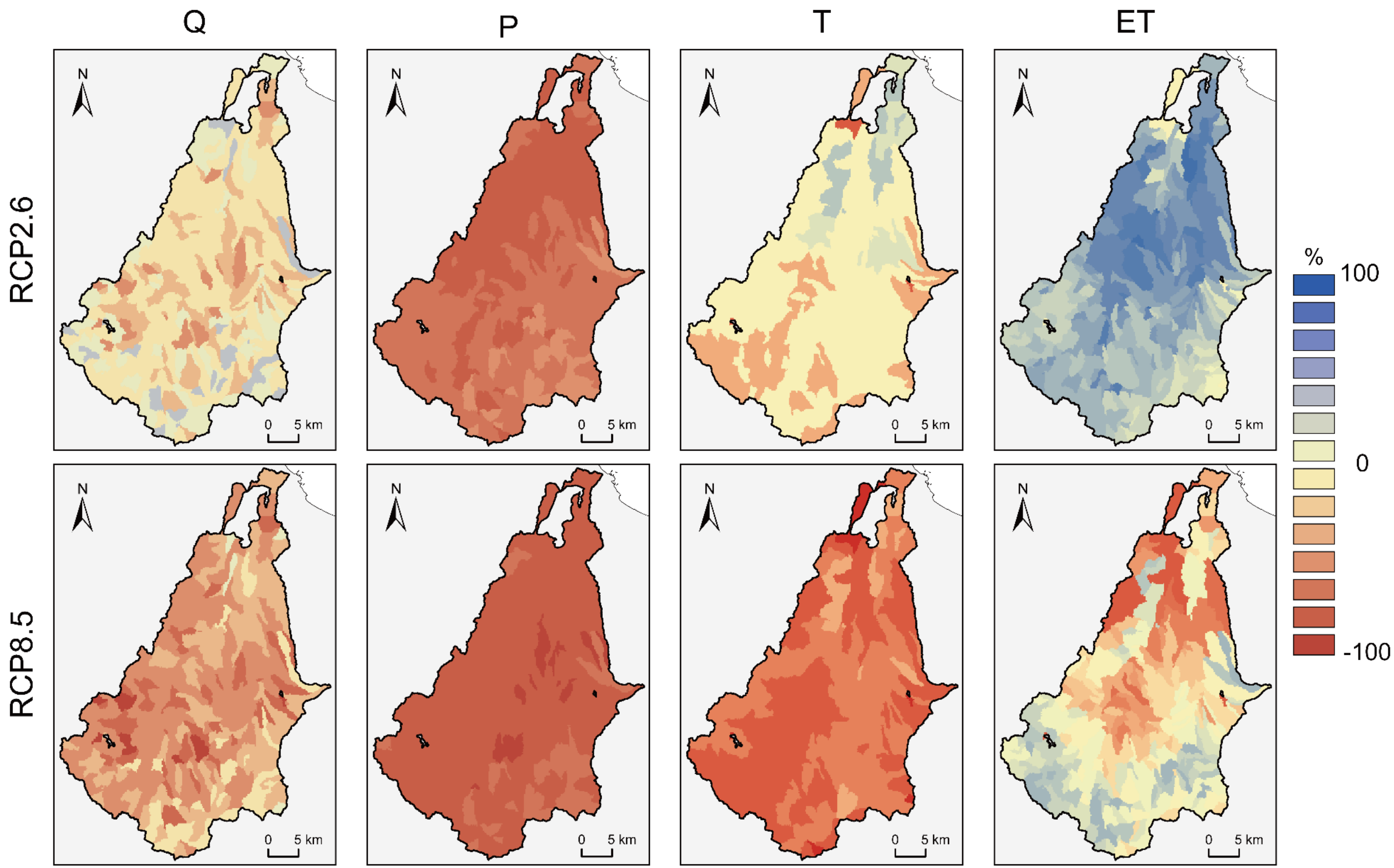

Fig. 12. Spatial distribution of relative change in streamflow (Q), precipitation (P), temperature (T), and evapotranspiration (ET) during winter in the two scenarios. Spatial distribution is displayed at the subbasin level. Relative change is described by percentage (%) compared to the present level. The color scheme corresponds to the water content variation in the water cycle.

Based on the results described in this section, primary implications are discussed as follows.

1. A possible drought in the future is one of the most concerning issues in response to climate change (Sheffield & Wood, 2011). In the present study, a significant decrease in the low flow and droughty flow in the RCO8.5 scenario, i.e., ΔQ_{clim} (10), may imply such an issue in the ARB. As a flow regime index, the droughty flow has a particular socioeconomic implication as the river flow at this level is commonly utilized in water use activities (Musiake et al., 1981). In one previous study, the likely change of droughty flow in Japan in 2075-2099 was discussed by simulating streamflow under the projected future climate (Tachikawa et al., 2011). A likely increase in droughty flow in Hokkaido was reported in the referred study, which is in contrast to the results of the present study (Fig. 8). The atmospheric general circulation model used by Tachikawa et al. (2011) was an earlier version of the same model used in the present study (MRI-AGCM3.2S, 20 km), while the latter was then regionally downscaled via the NHRCM05 to produce the JMA-GWP9. Therefore, the projected regional variation considered in the climate projection in the referred study might be less robust than that applied in the present study. Indeed, Sakata et al. (2016) conducted a more specific study on the change of specific droughty flow (the ratio of droughty flow over the catchment area at the given point) in future Hokkaido by analyzing the long-term historical change via a regional regression model. The future climate conditions were derived from the MIROC3.2 and JMA MRI-NHM models. The referred study reported that the specific droughty flow ($m^3 \cdot s^{-1} \cdot 100km^{-2}$) around the ARB region changed from 1.0-1.5 in 2001-2010 to 0.75-1.30 in the later decades of this century. This result is quantitatively comparable to the results in the present study, which are 0.98 in 2001-

2010 to 0.90 (RCP2.6) and 0.74 (RCP8.5) in 2076-2095. This degree of change suggests a higher risk of drought in the future and could be considered a warning sign for local basin management actions (Sakata et al., 2016). The results in the present study further support this concern in the ARB.

2. In addition to the change of droughty flow, the significant changes of streamflow in its quantity and pattern in the melting season, i.e., ΔQ_{clim} (4, 5), are concerning results to the water resource as well. For example, similar results were reported in the Ishikari River (Nakatsugawa, 2015; Usutani & Nakatsugawa, 2005). The referred studies showed that due to the acceleration of snowmelt caused by the projected temperature increase, streamflow of the Ishikari River in May and June decreased, while peak flow during the melting season shifted from late April to early April. The time shift is very similar to the results in the present study in the RCP8.5 scenario, i.e., ΔQ_{clim} (5). Nakatsugawa (2015) also compared the projected daily streamflow of the Ishikari River in April-June with the approximate irrigation water requirement in the region (expressed by the *water right*, or Suiriken in Japanese) and reported that the latter significantly exceeded the former during the comparison period. This comparison is because the paddy field's water use during its puddling stage depends critically on the streamflow from late April to June. Therefore, such a discrepancy means that the available river flow cannot satisfy the desirable water uptake. In the present study, the recorded water right near the Hongou station is nearly 8 $m^3 \cdot s^{-1}$ (Hokkaido Regional Development Bureau, 1994), which does not exceed the daily streamflow (Fig. 7) during the discussed period. However, the water right is not necessarily the maximum water uptake, and the actual value of the latter may vary around the

former (Maruyama, 1986). Therefore, considering that the streamflow during the period under RCP8.5 indeed significantly decreased compared to the present level, the risk of water use shortage could be considered inclined.

3. Besides the possible impacts on water resources, the fishery is another major socioeconomic component on which the streamflow variation may impact. Sugihara and Hirai (2015) conducted a study to extend the pre-established relationship between the reproductivity of Shijimi and the habitat properties (water temperature, salinity, dissolved oxygen level) to a relationship between the former and the streamflow changes. The interannual change of the median flow of the Sarobetsu River was compared to that of the catch number of Shijimi in the same region during 1980-2012. A negative correlation was found between the two, in which the correlation coefficient increased when a lag time by year between the two was applied (Sugihara & Hirai, 2015, Fig. 20). This is because the time by which Shijimi reaches its commercial size (the practical standard for the commercial catch) is usually around 9 to 10 years in the case of Teshio River (to which the Sarobetsu River contributes), and its growth can be affected by the growth rate of the newborn in the recent past years, which varies depending on the habitat condition of the present year (Sugihara & Hirai, 2015; Utoh, 1981). In the present study, the same comparison using a least square regression was conducted between the two components, i.e., the annual commercial catch of Shijimi in Lake Abashiri and the annual median flow at Hongou station during 1960-2008. Similar to the referred study, a negative correlation was found between the two components in the present study. Moreover, the correlation coefficient of the relationship increases when the lag time (year) is higher than three,

and becomes significant from seven (Fig. 13). It has been reported that the majority of Shijimi in Lake Abashiri takes five or six years to reach its commercial size, while the fast-growing individuals may take four (Watanabe et al., 2021). The timing adequately explains the result in Fig. 13. Therefore, considering the results in Fig. 8, a possible positive impact on the reproductivity of Shijimi in Lake Abashiri may be expected. However, it was also explained that increases in precipitation and temperature during July-September may suppress the short-term growth rate of Shijimi (Sugihara & Hirai, 2015). Consequently, a negative impact on the reproductivity of Shijimi in Lake Abashiri can be expected according to the projected climate (Fig. 9). Collectively, a likely less stable future for the capture of Shijimi was implied.

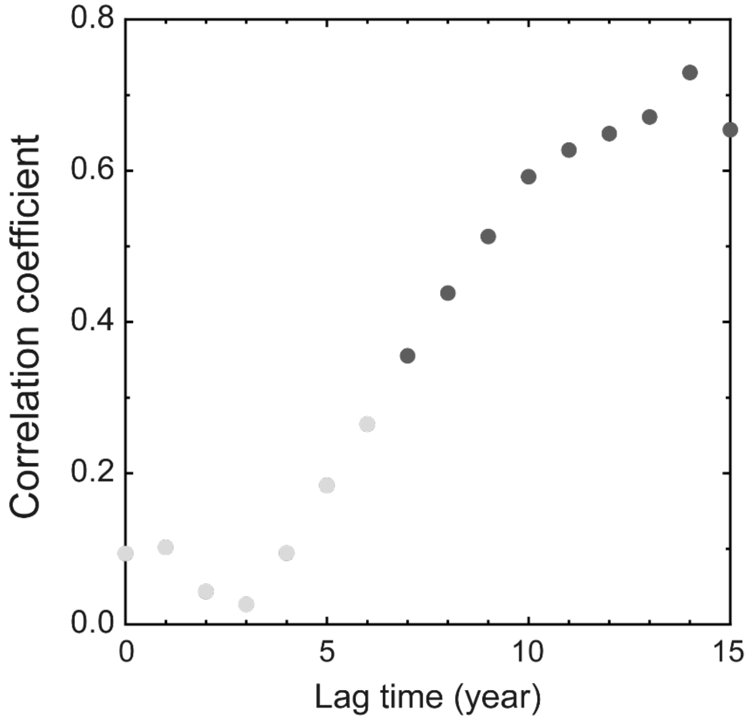

Fig. 13. Relationship between the annual median flow of the ARB and the annual commercial catch of Shijimi in Lake Abashiri in 1960-2008. The vertical axis is the correlation coefficient in the relationship; the horizontal axis is the lag time between the two components. A darker point denotes a significant correlation.

In the case of Shirauo, Hayano et al. (2013) compared the interannual change of its catch number in Lake Abashiri with that of the average daily streamflow of Abashiri River from August to November in 1985-2007. It was discovered that the former is considerably sensitive to the occurrence of higher streamflow, and that more frequent and heavier rainfall is likely to cause a negative impact on the catch number of Shirauo. As an increase in streamflow variability during July-August was found in both future scenarios, a likely less stable future for the capture of Shirauo was implied.

In the case of Wakasagi, Asami (2004) conducted a comprehensive study on its life ecology in Lake Abashiri and summarized a complex relationship between the growth of Wakasagi and numerous factors. It was explained that Wakasagi in Lake Abashiri experiences its larva stage (May-June) and juvenile stage (July-November) in the lake, where its growth rate is significantly related to the production of *Sinocalanus tenellus*, in addition to the water temperature, salinity, and Chlorophyll *a* concentration. The seaward migration occurs in July-November, followed by upstream migration by the end of December. The fish stays in the lake until April and begins its second and last year of life with a similar migration cycle. Fisheries activity in Lake Abashiri mainly primarily on production during January-March, which varies considerably from year to year (Asami, 2004). Therefore, the impact of the estimated streamflow change in the ARB on the productivity of Wakasagi was difficult to conclude, not only because its primary influencer, i.e., *Sinocalanus tenellus*, has a nonlinear relationship with the water temperature, but also because its migration number varies with the variation of its population density within the lake (Asami, 2004; Asami & Ito, 2003).

5.3 Streamflow under future LULC conditions

Averaged streamflow results were compared between the present time (2001-2005) and the five future scenarios (BaU, PC, PD, NC, ND; 2050). This section describes the LULC-induced streamflow change (ΔQ_{lulc}), marked by number for the convenience of reference in their corresponding interpretations. Same as in ΔQ_{clim}, the *significance* of change is indicated based on the *p*-value in the *t*-test, where a significant difference is noted when $p < 0.05$, and vice versa.

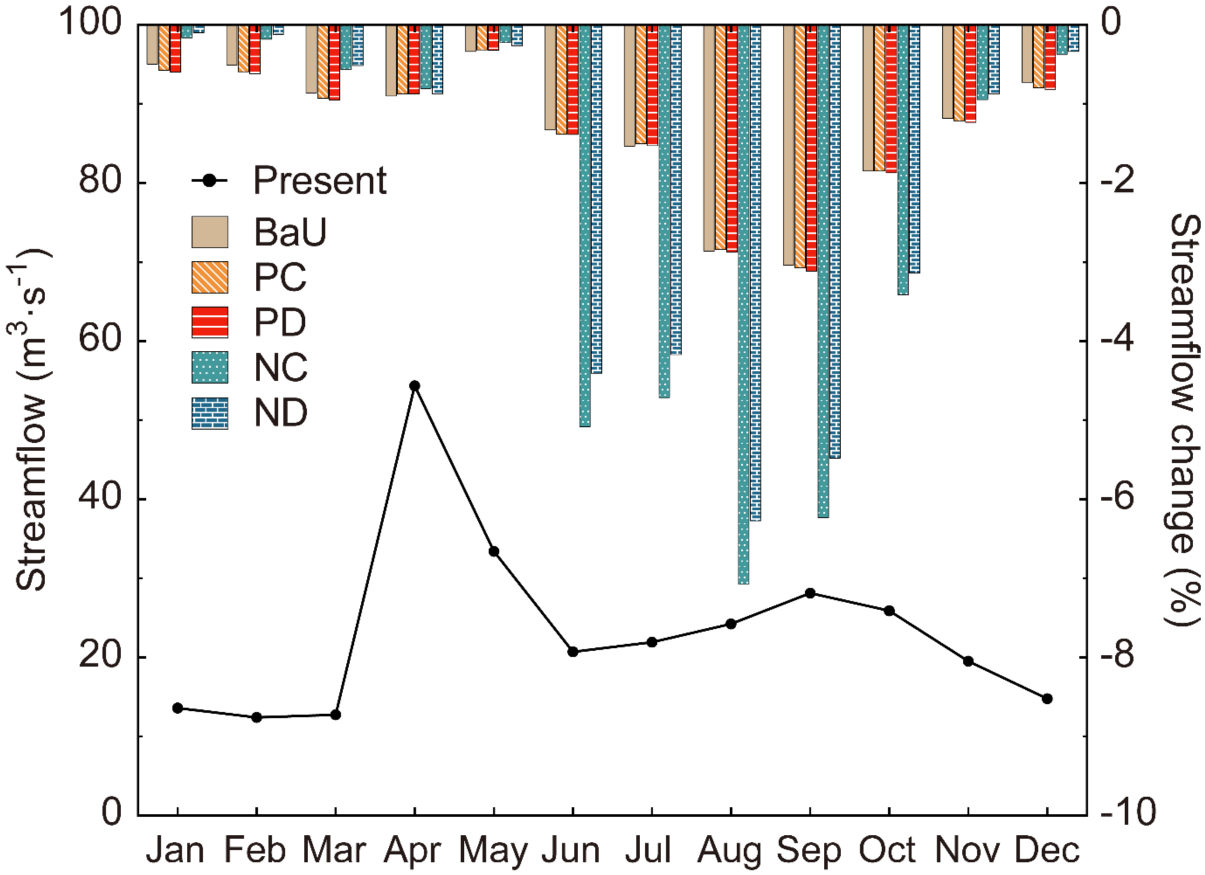

Fig. 14. Present streamflow (2001-2005) and the relative change in each future LULC scenario (2050). The left axis and the line are present streamflow; the right axis and column are relative change compared to the present streamflow. Future streamflow was not shown due to visually unnoticeable difference.

Between the present and future streamflow results, (1) an insignificant decrease was found in every month and in each scenario (Fig. 14). On the other hand, between the relative change in the two natural capital-based scenarios (NC, ND) and the other three scenarios (BaU, PC, PD), significant differences were found, except in May and June. More specifically, (2) the former is significantly lower than the latter in November-March; and (3) the former is significantly higher than the latter in June-October.

Between the present and future streamflow results, the LULC conditions (Figs. 2, 4a) were the only source of difference. ΔQ_{lulc} (1) most likely resulted from the insignificant increase of forest coverage (Table 2), which changed from 68.1% in the present to 71.8%, 71.7%, 71.7%, 70.8%, and 70.9% in the five scenarios. Nevertheless, the increase in forest coverage can lead to an increase in ET and hence the streamflow decrease. ΔQ_{lulc} (2) is likely related to the change in forest coverage as well, but through different process. SWAT calculation considers the dormancy of trees by effectively excluding the canopy interception of deciduous trees in winter. Table 2 shows that the coverage of evergreen trees is the same between the five scenarios. Therefore, ΔQ_{lulc} (2) cannot be explained directly by the change in forest coverage. On the other hand, Fig. 2 shows that the reduced grassland coverage was replaced with deciduous broadleaf tree. Such a transformation can cause a decrease in the surface albedo within the area, and hence an increase in ET, then a decrease in streamflow. Therefore, the more significant transformation of grassland in BaU, PC, and PD likely led to difference in ΔQ_{lulc} (2). Lastly, ΔQ_{lulc} (3) is explained by the significant increase in paddy field coverage, where it increased by 150% in BaU, PC, and PD, and by more than 500% in NC and ND. More specifically, the change in the paddy field led to a change in its water demand, calculated based on its area, as introduced in section 4.4. In addition, the built-up area in NC and ND is significantly different from the other three scenarios, which may also lead to a change in the water demand. However, the domestic water use in the ARB is not taken from the river channel but directly from groundwater instead (https://www.city.abashiri.hokkaido.jp/280josuido/), its representation was not included in the streamflow simulations considering the paucity of applicable information.

Based on the results described in this section, the primary implication is that under a conservatively projected future, LULC in the ARB may not significantly impact the local streamflow. This implication is comparatively different than what has been reported in many previous studies (e.g., Schilling et al., 2008; Tao et al., 2014; Wijesekara et al., 2012). However, much more extreme transitions of LULC distributions were commonly given in these studies. For example, Kayitesi et al. (2022) reviewed studies conducted in tropical regions and reported that a majority of the studies (68%) focused on the area where significant deforestation occurred or was expected to occur. The tendency was expected to be maintained in the near future. It was also summarized that significant streamflow and surface runoff changes were mostly reported in studies where a substantial change in forest coverage or agricultural land coverage was considered (Kayitesi et al., 2022, Table 1). Cuo (2016) reviewed studies on this topic conducted in mesoscale basins worldwide, and reported a similar tendency in the magnitude of LULC changes (Cuo, 2016, Table 6.1). Nevertheless, both review studies concluded that LULC changes do not necessarily lead to an essential change in streamflow, and suggested that more specific changes, such as dam construction or river morphology alteration, could deliver more noticeable changes to the streamflow. However, reasonable prediction on such changes is difficult to produce without any additional information from the related stakeholders. Therefore, considering the projected LULC conditions in the present study, it is reasonable to expect an insignificant corresponding change in the future streamflow in the ARB. Additionally, simulations in combined future climate and LULC conditions were also conducted in the present study. However, no significant difference was produced compared to the simulation in which the same climate condition was applied. Such results were therefore omitted.

6. Discussion

6.1 Significance of the empirical approach

As explained in section 4.3, the empirical approach aims to minimize the use of statistical tuning, and it is essentially a sophistication to the current parameter determination manner in SWAT. It is important to note that the data limitation is the crucial premise herein; otherwise, the parameters could be realistically determined based on the in-situ measurements. When facing a data limitation, the tuning in SWAT is conventionally considered preferable over the empirical approach in previous studies, because the latter is deemed impractical and unnecessary. However, the model performance was significantly improved after the empirical approach (Fig. 15). Compared to the observation, the discrepancy in the initial simulation was successfully reduced in the modified simulation, and reached a statistically acceptable model performance. The conventional manner would require applying the tuning on a model performance similar to the initial simulation until the discrepancy is remedied. However, as explained in section 4.3.1, such a practice would lead to significant uncertainties yielded by the cross-compensation effect, resulting in highly conditional model performance, unsuitable for predictive applications. Therefore, the result in Fig. 15 effectively supports the practicality and necessity of the empirical approach without the contribution from direct measurements or tuning.

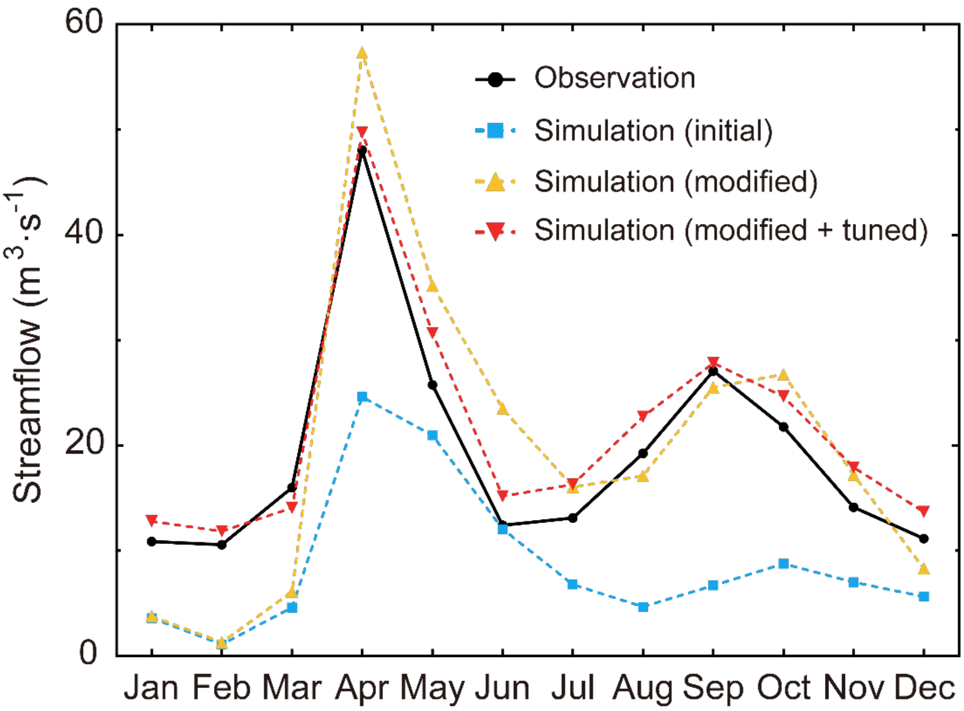

Fig. 15. Comparison between the streamflow in observation and simulations at Hongou station in 2001-2005. Parameter values in the simulation were left as default (initial), modified in the empirical approach (modified), and tuned after being modified in the empirical approach (modified + tuned), respectively.

Furthermore, the necessity of the empirical approach under a data limitation is commonly opposed by the notion that its effect cannot be directly verified by observation, regardless of the efforts. However, this study argues that an opposite consideration should be given instead. Namely, precisely because of the paucity of in-situ observation, a physically meaningful determination process for the parameters is necessary. In addition to the logical reasons proposed in section 4.3, three practical advancements in this study, as compared to the previous studies, contribute to the necessity of the empirical approach.

1. The selection of parameters for tuning became more physically reasonable. Due to the large number of parameters, only a selective portion must be used for tuning, while the rest is left unchanged from its default value. However, such a parameter selection manner can become problematic, especially under a data limitation, as it is conventionally based on subjective reasons such as tested sensitivity and the modeler's experience. For example, van Griensven et al. (2012) reviewed numerous SWAT applications conducted in the upper Nile River basin, in which the number of tuned parameters varies widely between different studies: Mulungu and Munishi (2007) used more than ten parameters (CN2, ALPHA_BF, SURLAG, SOL_AWC, CH_K, CH_N, CANMX, REVAPMN, SOL_ALB and others), Kingston and Taylor (2010) used ten parameters (CH_K, CH_N, SURLAG, SOL_AWC, CANMX, ESCO, CN2, SOL_Z, SOL_ALB, GWQMN), Setegn et al. (2008) used eight parameters (ESCO, CN2, ALPHA_BF, REVAPMN, SOL_AWC, GW_REVAP, CH_K2, GWQMN), Mekonnen et al. (2009) used eight parameters (CN2, SURLAG, GW_DELAY, SOL_AWC, SOL_Z, ALPHA_BF, GW_REVAP, REVAPMN), while Jayakrishnan et al. (2005) and Tibebe and Bewket (2011) used only two parameters (SOL_AWC and ESCO, CN2 and ESCO, respectively). The sensitivity of the tuned parameters was used as the reason for the parameter selection in every

study (van Griensven et al., 2012). However, except for the inclusion of a few generally sensitive parameters, such as CN2 and SOL_AWC, the decision on the parameter selection is substantially different between different studies conducted in the same river basin system. Such differences suggest that even though a satisfactory agreement between the simulation and observation may be achieved via tuning, the model performance could be highly conditional to the tuning period. In contrast, the four tuned parameters in this study (SFTMP, SMTMP, SOL_AWC, GW_DELAY) were chosen without considering their statistical sensitivity. The four parameters were deemed necessary for tuning mostly because no comparable reference in the ARB could be found for the empirical approach, in addition to their physical involvement in the water cycle. While the use of tuning is inevitable, especially under limited data availability, the empirical approach allows the parameters for tuning to be selected in a more physically reasonable and less performance-focused manner.

2. The numerical values of the tuned parameters became more physically meaningful. As explained in section 4.3.1, the compensation effect can easily lead to physically unrealistic parameter values, regardless of the model performance. This negative impact becomes particularly distinct when the tuning pressure is considered significant. For example, in the author's previous study regarding the river basins in the Kamchatka Peninsula (KP), Russia (Shi et al., 2021), the only available observation was monthly streamflow data of several rivers. SWAT was the primary tool to extend the limited observation to other ungauged basins in the KP. A high tuning pressure was expected due to the extreme data limitation. Consequently, some tuned parameters showed unrealistic physical meaning after the process. For example,

SFTMP (°C, snowfall threshold temperature) was tuned as higher than 10 or lower than −10 in several river basins (Shi et al., 2021, Table A2). In contrast, the SFTMP was tuned to 3.2 in the present study. Jennings et al. (2018) reported the same value in this region as 3.6 using a binary logistic regression phase-prediction model based on a comprehensive 29-year meteorological observation dataset. Another tuned parameter in the present study, SOL_AWC (%, available water capacity), was tuned to an overall increase from its default values. The change is reasonable as a large portion of the ARB is covered by Andosols (Fig. 4b), a volcanic soil type typically with considerable water retention capacity (Obara et al., 2011). Spilling (2018) conducted an extensive study on the variation of soil hydraulic properties, and concluded that the available water capacity tends to become more prominent in less steep areas, which also agrees with the topographic condition in the ARB. In contrast to the non-physical nature of tuning, in which the physical meaning of parameters cannot be warranted, the reduced tuning pressure due to the empirical approach successfully suppressed this issue. In addition, this advancement could, in turn, improve the reliability of the calculations in which the tuned parameters directly involve, i.e., snowmelt, soil water content, and groundwater release.

3. The empirical approach improves the physical meaning of both the untuned parameters (directly) and the tuned parameters (indirectly). The physical meaningful sophistication of SWAT led to the third practical advancement compared to the previous studies, i.e., the suppressed model performance reduction. A *perfect* model performance of a hydrological model is never possible, as a certain degree of generalization and simplification is always involved, regardless of the model's purpose. Therefore, its performance will inevitably reduce

when the tuned model is reapplied to a different spatial or temporal setting. The former is utilized in the predictions in ungauged basins (PUB), and the latter is utilized in model validations. For example, using SWAT, Liu et al. (2022) assessed the impacts of climate and LULC changes in western China. The tuning was conducted in 1976-1999, and an NSE of 0.7 was achieved. In contrast, the validation was conducted in 2001-2019, and the model performance became questionable (Liu et al., 2022, Figs. 6 and 7). Studies that focused on modelling previous streamflow events tend to conduct validation in much shorter period to demonstrate desirable performance (e.g., Kalin & Hantush, 2006; Tolson & Shoemaker, 2007). In the case of PUB, the tuned model is reapplied to a different spatial setting, while the temporal setting should be left unchanged. For instance, Shi et al. (2021) initially tuned the parameters in 1984-2013 in several gauged basins, then reapplied the parameters from the gauged basins to their respective neighboring ungauged basins and performed simulation again in 1984-2013. This practice was to extend the limited data to allow conditionally reasonable simulation in ungauged basins. While simulations in the ungauged basins cannot be validated, the model performance declined by nearly 40% in a few cases in the validation (Shi et al., 2021, Table 3). In both practices, a critical premise is that the difference between the spatiotemporal setting in which the model was tuned and that to which the model is reapplied should be considered insignificant, or otherwise, the reapplied simulation would become ineffectual to its purpose. Despite the limited data available in this study, the performance reduction was not overly significant to compromise the model even at the daily scale (Table 6). The suppressed reduction of model performance is owing to the overall improvements in the physical meaning of the parameters.

In addition to the three advancements discussed above, it is worth noting that despite the effort to minimize tuning, the primary intention in this study was not to reject the significance of tuning but rather, to emphasize its use in a more physically reasonable manner as a new insight to SWAT applications. More specifically, the results in this study show that it is necessary and meaningful to apply different parameters with different physical meanings in response to the specific target basin, in contrast to the conventional manner where the significance of commonly insensitive parameters is commonly ignored, and vice versa. This point is widely overlooked in the existing SWAT applications. For example, through the extensive literature review to realize the empirical approach, the author noticed that CANMX (canopy storage capacity) is one of the most frequently misused parameters in SWAT applications. Its involvement in the calculation is only active when the Green-Ampt infiltration method is used rather than the Curve Number method. However, numerous studies included CANMX during their tuning process, even though the Green-Ampt infiltration method was not used in the calculations. This mistake is frequently presented even in highly ranked journals (e.g., Grusson et al., 2015; Herman et al., 2018; Shimizu et al., 2013; van Griensven et al., 2006), which demonstrates how conventional mistakes hidden in the model preparation process can be easily overlooked provided that satisfactory final performance was achieved.

6.2 Remaining limitations

The present study aims to produce streamflow estimations under limited data availability by using a hydrological model. While this key objective was achieved by focusing on the physical sophistication of the model, several remaining limitations in this study are worth noting from a more general perspective.

1. As mentioned in chapter 4, the meteorological input dataset differed between the present streamflow simulation (DSJRA-55) and the future climate-induced simulation (JMA-GWP9). More specifically, while the same non-hydrostatic model (Saito et al., 2006) was used for the downscaling process, the boundary conditions were different, i.e., reanalysis data in the DSJRA-55, and AGCM-simulated data in the JMA-GWP9. The difference in the boundary condition could lead to a systematic difference between the two meteorological inputs, which may lead to an additional difference in the streamflow results. For example, the present streamflow showed a quantitatively insignificant difference at the beginning of the melting season compared to the two future results (Fig. 7a). The present streamflow began to increase nearly a week earlier than the two future streamflow results. By comparing the meteorological inputs, it was found that while no significant difference existed in the temperature data in the discussed period, the precipitation began to increase approximately four days earlier in the DSJRA-55 than in the JMA-GWP9. The difference might be the consequence of using different meteorological datasets. Nevertheless, the primary reason for applying different datasets was the concern over the accuracy of each dataset during the model preparation process. More specifically, in the case of DSJRA-55, the regional bias was comprehensively evaluated and corrected before the release of the dataset (Kayaba et al., 2016). In contrast, the systematic bias in the released version of JMA-GWP9 was intentionally left uncorrected to allow individual correction by the data users according to their specific target location (https://www.data.

jma.go.jp/cpdinfo/GWP/Vol9/pdf/gwp9_manual.pdf). Bias correction for the JMA-GWP9 was indeed conducted in this study using the least square linear regression, which is a relatively simple process. The simplicity may not lead to a significant problem in future streamflow simulations, as most of the results were discussed monthly. However, the simplicity could function as an additional uncertainty in the tuning process, which can be hidden by the compensation effect after applying the tuning. Therefore, using the DSJRA-55 during the model preparation process was considered preferable, even though it may contain an essential difference from the JMA-GWP9. Nevertheless, a more robust bias correction on the JMA-GWP9 could be considered a solution to allow a unanimous use of meteorological input between the present and future simulations.

2. Compared to the streamflow simulation in the present, changing factors were rigorously controlled in future simulations. More specifically, only climate or LULC conditions were altered, while all the remaining inputs and parameters were left unchanged (except the water use demand of the paddy field, which varied in response to the paddy field area). The rigorous control allows a straightforward interpretation of the reason for streamflow changes. However, it also assumes no interconnection between the LULC change and climate change, which is not necessarily realistic depending on the significance of the change. For example, LULC change in the form of significant deforestation was reported to have caused a decrease in winter precipitation in Hokkaido in the recent past (Sugimoto et al., 2015a). In the referred study, sensitivity analysis revealed that deforestation led to an increase in snow cover and surface albedo, which altered the regional surface energy budget and ultimately caused a decrease in

winter precipitation. Furthermore, the referred study also suggested a change in the regional wind speed as another consequence of deforestation. In addition to deforestation, a strong influence was found from the historical urbanization in southwestern Hokkaido to the daily temperature in winter at a local scale (Sugimoto et al., 2015b). Based on the projected future conditions in the present study, excluding such interconnections between the LULC change and climate change could be considered acceptable, as neither the forest coverage nor the built-up area showed significant change relative to the present level. On the other hand, adopting such details to the present study could improve its general applicability in future applications. A meaningful insight suggested from this remaining limitation is that a combination of multiple methods on the future streamflow estimation, i.e., paired catchments, statistics-based analysis, and physical hydrological modeling, could be a challenging and meaningful continuity of the present study in the future.

7. Conclusions

In this study, the primary challenge and research target was to produce reliable future streamflow estimations using a hydrological model under limited data availability. A semi-distributed hydrological model, SWAT, was applied to the Abashiri River basin (ARB) under a series of future climate and LULC conditions. Estimated future streamflow of the ARB showed:

1. A significant decrease during the melting season, resulted from a significant decrease in winter precipitation.

2. A significant two-week early shift of the peak flow occurrence and a significant decrease in early summer, resulted from significantly increased temperature.
3. A high variability with a likely increase in the quantity during autumn, resulted from highly variable precipitation.
4. A difference in the winter spatial distribution between the future scenarios, resulted from a mixed impact of precipitation and temperature.
5. An insignificant decrease throughout the year compared to the present level, resulted from slightly increased forest coverage.
6. A significant difference in the relative change in midsummer, autumn, and winter, resulted from a significant difference between the LULC change in the future scenarios.

While future LULC in the ARB may affect streamflow less significantly than the impact of climate change, an increasing risk of irrigation water shortage was suggested in both cases. In addition, a less stable condition for the fishery activities in Lake Abashiri was implied. To ensure the reliability of streamflow estimations, a consistent and physically meaningful sophistication on the parameter determination process was proposed and realized in SWAT, in which the chief intention was to minimize statistical tuning. The model simulation was successfully prepared and validated, by which the above future streamflow results were derived. In contrast to the conventional use of SWAT, this study demonstrated the practicality and necessity of minimizing the statistical tuning in SWAT when facing limited data availability. The method and results could serve as an emphasis on the physically meaningful sophistication of SWAT, particularly in its predictive applications.

Acknowledgements

I want to express my most profound appreciation to Dr. Takayuki Shiraiwa, who led me into the proper academic world and has been the supervisor for my entire career as a graduate student. Dr. Shiraiwa's constant enthusiasm, rigorous attitude, and "brutal" honesty toward science changed me as a student, as a researcher, and as a person. I also extend my most sincere appreciation to Dr. Takeo Onishi and Dr. Hideaki Shibata, who introduced the SWAT model (the primary tool I used in my M.S. and Ph.D. studies) to me and provided countless help and guidance since then. I must also thank Dr. Humio Mitsudera and Dr. Tomonori Sato, who frequently offered me insightful knowledge and advice from different aspects outside my own expertise. Completing this study would not have been possible without the support from any of the five persons above. I am indebted to Ms. Xin Peng for her unconditional assistance and support. I am grateful to Mr. Yutaka Kurosaki for his critical help in the data acquisition of this study. I am thankful to Dr. Osamu Saito for providing the LULC projection data. I am also grateful to Mr. Takaaki Watanabe for the information he supplied on basin management in Abashiri City. Special thanks to the Digital Collections & Archives of Tufts University for providing one critical reference used in this study. Lastly, I would like to express my unparalleled gratitude to my family, without whom none of my success would be possible.

This study was partly supported by Grants-in-Aid for Scientific Research (B), Japan Society for the Promotion of Science (JSPS KAKENHI), Grant Number JP21H01154.

References

Abbaspour, K. C. (2015). *SWAT-CUP: SWAT Calibration and Uncertainty Programs—A User Manual*. Swiss Federal Institute of Aquatic Science and Technology, EAWAG, Dübendorf, Switzerland.

Abbaspour, K. C. (2022). The fallacy in the use of the "best-fit" solution in hydrologic modeling. *Science of The Total Environment*, *802*, 149713. doi.org/10.1016/j.scitotenv.2021.149713

Abbaspour, K. C., Rouholahnejad, E., Vaghefi, S., Srinivasan, R., Yang, H., & Kløve, B. (2015). A continental-scale hydrology and water quality model for Europe: Calibration and uncertainty of a high-resolution large-scale SWAT model. *Journal of Hydrology*, *524*, 733–752. doi.org/10.1016/j.jhydrol.2015.03.027

Abbaspour, K. C., Vaghefi, S. A., & Srinivasan, R. (2018). A Guideline for Successful Calibration and Uncertainty Analysis for Soil and Water Assessment: A Review of Papers from the 2016 International SWAT Conference. *Water*, *10*(1), Article 1. doi.org/10.3390/w10010006

Aich, V., Liersch, S., Vetter, T., Huang, S., Tecklenburg, J., Hoffmann, P., Koch, H., Fournet, S., Krysanova, V., Müller, E. N., & Hattermann, F. F. (2014). Comparing impacts of climate change on streamflow in four large African river basins. *Hydrology and Earth System Sciences*, *18*(4), 1305–1321. doi.org/10.5194/hess-18-1305-2014

Akasaka, M., Takenaka, A., Ishihama, F., Kadoya, T., Ogawa, M., Osawa, T., Yamakita, T., Tagane, S., Ishii, R., Nagai, S., Taki, H., Akasaka, T., Oguma, H., Suzuki, T., & Yamano, H. (2014). Development of a National Land-Use/Cover Dataset to Estimate Biodiversity and Ecosystem Services. In S. -ichi Nakano, T. Yahara, & T. Nakashizuka (Eds.), *Integrative Observations and Assessments* (pp. 209–229). Springer Japan. doi.org/10.1007/978-4-431-54783-9_10

Anderson, E. A. (1976). *A Point Energy and Mass Balance Model of a Snow Cover*. U.S. Department of Commerce, National Oceanic and Atmospheric Administration, National Weather Service, Office of Hydrology.

Arcement, G. J., & Schneider, V. R. (1989). *Guide for selecting Manning's roughness coefficients for natural channels and flood plains*. doi.org/10.3133/wsp2339

Arnold, J. G., Kiniry, J. R., Srinivasan, R., Williams, J. R., Haney, E. B., & Neitsch, S. L. (2012). *Soil and Water Assessment Tool, Input/Output Documentation, ver. 2012.* Texas Water Resources Institute, Texas, USA.

Arnold, J. G., Moriasi, D. N., Gassman, P. W., Abbaspour, K. C., White, M. J., Srinivasan, R., Santhi, C., Harmel, R. D., van Griensven, A., Van Liew, M. W., Kannan, N., & Jha, M. K. (2012). Swat: Model Use, Calibration, and Validation. *Transactions of the Asabe*, *55*(4), 1491–1508.

Arnold, J. G., Srinivasan, R., Muttiah, R. S., & Williams, J. R. (1998). Large Area Hydrologic Modeling and Assessment Part I: Model Development1. *JAWRA Journal of the American Water Resources Association*, *34*(1), 73–89. doi.org/10.1111/j.1752-1688.1998.tb05961.x

Asami, H. (2004). *Early life ecology of Japanese smelt (Hypomesus nipponensis) in Lake Abashiri, a brackish water, estern Hokkaido, Japan* (No. 67; pp. 1–79). Hokkaido Fisheries Experimental Station.

Asami, H., & Ito, Y. (2003). Population dynamics and estimated production of Sinocalαnus tenellus (Kikuchi) (Copepoda: Calanoida) in a brackish-water environment, Lake Abashiri, eastern Hokkaido, Japan. *Bulletin of the Plankton Society of Japan*, *50*(2), 67–78.

Atkinson, P. M., & Tatnall, A. R. L. (1997). Introduction Neural networks in remote sensing. *International Journal of Remote Sensing*, *18*(4), 699–709. doi.org/10.1080/014311697218700

Attarod, P., Sadeghi, S. M. M., Pypker, T., Bagheri, H., Bagheri, M., & Bayramzadeh, V. (2014). Needle-leaved trees impacts on rainfall interception and canopy storage capacity in an arid environment. *New Forests*, *46*. doi.org/10.1007/s11056-014-9464-2

Balascio, C. C., Palmeri, D. J., & Gao, H. (1998). Use of a genetic algorithm and multi-objective programming for calibration of a hydrologic model. *Transactions of the ASAE (USA)*. doi.org/10.13031/2013.17229

Barnett, T. P., Adam, J. C., & Lettenmaier, D. P. (2005). Potential impacts of a warming climate on water availability in snow-dominated regions. *Nature*, *438*(7066), Article 7066. doi.org/10.1038/nature04141

Biodiversity Center of Japan. (1991). *4th Natural Environment Survey on Inland Waters*. Ministry of the Environment.

Bosch, J. M., & Hewlett, J. D. (1982). A review of catchment experiments to determine the effect of vegetation changes on water yield and evapotranspiration. *Journal of Hydrology*, *55*(1), 3–23. doi.org/10.1016/0022-1694(82)90117-2

Brown, A. E., Zhang, L., McMahon, T. A., Western, A. W., & Vertessy, R. A. (2005). A review of paired catchment studies for determining changes in water yield resulting from alterations in vegetation. *Journal of Hydrology*, *310*(1), 28–61. doi.org/10.1016/j.jhydrol.2004.12.010

Brunt, D. (1932). Notes on radiation in the atmosphere. I. *Quarterly Journal of the Royal Meteorological Society*, *58*(247), 389–420. doi.org/10.1002/qj.49705824704

Brunt, D. (1952). *Physical and Dynamical Meteorology* (2nd ed.). Cambridge University Press.

Brutsaert, W. (2005). *Hydrology: An Introduction* (Illustrated edition). Cambridge University Press.

Bulygina, N., McIntyre, N., & Wheater, H. (2011). Bayesian conditioning of a rainfall-runoff model for predicting flows in ungauged catchments and under land use changes. *Water Resources Research*, *47*(2). doi.org/10.1029/2010WR009240

Bulygina, N., McIntyre, N., & Wheater, H. (2013). A comparison of rainfall-runoff modelling approaches for estimating impacts of rural land management on flood flows. *Hydrology Research*, *44*(3), 467–483. doi.org/10.2166/nh.2013.034

Cassel, D. K., & Nielsen, D. R. (1986). Field Capacity and Available Water Capacity. In *Methods of Soil Analysis* (pp. 901–926). John Wiley & Sons, Ltd. doi.org/10.2136/sssabookser5.1.2ed.c36

Changnon, S. A., & Demissie, M. (1996). Detection of changes in streamflow and floods resulting from climate fluctuations and land use-drainage changes. *Climatic Change*, *32*(4), 411–421. doi.org/10.1007/BF00140354

Chow, V., Maidment, D., & Mays, L. (1988). *Applied Hydrology* (1st edition). McGraw-Hill Science/Engineering/Math.

Costa, M. H., Botta, A., & Cardille, J. A. (2003). Effects of large-scale changes in land cover on the discharge of the Tocantins River, Southeastern Amazonia. *Journal of Hydrology*, *283*(1), 206–217. doi.org/10.1016/S0022-1694(03)00267-1

Croitoru, A.-E., & Minea, I. (2015). The impact of climate changes on rivers discharge in Eastern Romania. *Theoretical and Applied Climatology*, *120*(3), 563–573. doi.org/10.1007/s00704-014-1194-z

Cuo, L. (2016). Land Use/Cover Change Impacts on Hydrology in Large River Basins. In *Terrestrial Water Cycle and Climate Change* (pp. 103–134). American Geophysical Union (AGU). doi.org/10.1002/9781118971772.ch6

Downer, C., & Ogden, F. (2006). *Gridded Surface Subsurface Hydrologic Analysis (GSSHA) User's*

Manual; Version 1.43 for Watershed Modeling System 6.1. 221.

Engman, E. T. (1986). Roughness Coefficients for Routing Surface Runoff. *Journal of Irrigation and Drainage Engineering*, *112*(1), 39–53. doi.org/10.1061/(ASCE)0733-9437(1986)112:1(39)

Ficklin, D. L., Luo, Y., Luedeling, E., & Zhang, M. (2009). Climate change sensitivity assessment of a highly agricultural watershed using SWAT. *Journal of Hydrology*, *374*(1), 16–29. doi.org/10.1016/j.jhydrol.2009.05.016

Forestry Agency of Japan. (2013). *Forest Ecosystme Biodiversity Basic Survey (Shinrin seitaikei tayousei kiso chousa)*. Ministry of Agriculture, Forestry and Fisheries.

Gascón, E., Hewson, T., & Haiden, T. (2018). Improving Predictions of Precipitation Type at the Surface: Description and Verification of Two New Products from the ECMWF Ensemble. *Weather and Forecasting*, *33*(1), 89–108. doi.org/10.1175/WAF-D-17-0114.1

Gassman, P. W., Sadeghi, A. M., & Srinivasan, R. (2014). Applications of the SWAT Model Special Section: Overview and Insights. *Journal of Environmental Quality*, *43*(1), 1–8. doi.org/10.2134/jeq2013.11.0466

Grusson, Y., Sun, X., Gascoin, S., Sauvage, S., Raghavan, S., Anctil, F., & Sáchez-Pérez, J.-M. (2015). Assessing the capability of the SWAT model to simulate snow, snow melt and streamflow dynamics over an alpine watershed. *Journal of Hydrology*, *531*, 574–588. doi.org/10.1016/j.jhydrol.2015.10.070

Gupta, H. V., Kling, H., Yilmaz, K. K., & Martinez, G. F. (2009). Decomposition of the mean squared error and NSE performance criteria: Implications for improving hydrological modelling. *Journal of Hydrology*, *377*(1), 80–91. doi.org/10.1016/j.jhydrol.2009.08.003

Haines, A. T., Finlayson, B. L., & McMahon, T. A. (1988). A global classification of river regimes.

Applied Geography, *8*(4), 255–272. doi.org/10.1016/0143-6228(88)90035-5

Hamilton, S. (2007). Completing the loop: From data to decisions and back to data. *Hydrological Processes*, *21*(22), 3105–3106. doi.org/10.1002/hyp.6860

Hashizume, H., Nakata, G., Shinzato, T., Takikawa, S., Somego, M., & Uchimura, E. (1993). *Illustrated Practical Dendrology*. Asakura Publishing Co., Ltd.

Hayano, H., Miyakoshi, Y., Mano, S., Tamura, R., Kudo, H., & Kaeriyama, M. (2013). Temporal change in catches and resources of icefish *Salangichthys microdon* in Lake Abashiri, eastern Hokkaido, Japan. *Nippon Suisan Gakkaishi*, *79*(3), 372–382. doi.org/10.2331/suisan.79.372

Herman, M. R., Nejadhashemi, A. P., Abouali, M., Hernandez-Suarez, J. S., Daneshvar, F., Zhang, Z., Anderson, M. C., Sadeghi, A. M., Hain, C. R., & Sharifi, A. (2018). Evaluating the role of evapotranspiration remote sensing data in improving hydrological modeling predictability. *Journal of Hydrology*, *556*, 39–49. doi.org/10.1016/j.jhydrol.2017.11.009

Hirayama, S., Tadono, T., Ohki, M., Mizukami, Y., Nasahara, K. N., Imamura, K., Hirade, N., Ohgushi, F., Dotsu, M., & Yamanokuchi, T. (2022). Generation of High-Resolution Land Use and Land Cover Maps in JAPAN Version 21.11. *Journal of The Remote Sensing Society of Japan*, *42*(3), 199–216. doi.org/10.11440/rssj.42.199

Hokkaido Electric Power Company, & Sapporo Regional Headquarters of Japan Meteorological Agency. (1959). *Basic snow cover survey, study of snow melting (Sekisetsu kiso chōsa, yūsetsu no kenkyū)*. Hokkaido Electric Power Company et al. doi.org/10.11501/1378471

Hokkaido Regional Development Bureau. (1994). *History of river management in the Abashiri River (Abashirigawa chisuishi)*. Hokkaido Development Association.

Hong, S. Y., Minasny, B., Han, K. H., Kim, Y., & Lee, K. (2013). Predicting and mapping soil available water capacity in Korea. *PeerJ*, *1*, e71. doi.org/10.7717/peerj.71

Horie, T. (2004). *Fundamentals of Crop Cultivation (Sakumotsu saibai no kiso)*. Rural Culture Association Japan.

Hornberger, G. M., Wiberg, P. L., Raffensperger, J. P., & D'odorico, P. (2014). *Elements of Physical Hydrology* (2nd edition). Johns Hopkins Univ Pr.

Huber, W. C., & Dickinson, R. E. (1988). *Storm water management model, version 4: User's manual*. U.S. Environmental Protection Agency, Georgia, USA.

Japan Society of Civil Engineers. (2019). *Collection of Hydrualic Formulas (Suiri koushikishu)*. Maruzen Publishing Co., Ltd.

Jayakrishnan, R., Srinivasan, R., Santhi, C., & Arnold, J. G. (2005). Advances in the application of the SWAT model for water resources management. *Hydrological Processes*, *19*(3), 749–762. doi.org/10.1002/hyp.5624

Jennings, K. S., Winchell, T. S., Livneh, B., & Molotch, N. P. (2018). Spatial variation of the rain–snow temperature threshold across the Northern Hemisphere. *Nature Communications*, *9*(1), Article 1. doi.org/10.1038/s41467-018-03629-7

Jensen, M. E., Burman, R. D., & Allen, R. G. (1990). *Evapotranspiration and Irrigation Water Requirements* (1st ed.). ASCE Manuals and Reports on Engineering Practices No. 70.

Kalin, L., & Hantush, M. M. (2006). Hydrologic Modeling of an Eastern Pennsylvania Watershed with NEXRAD and Rain Gauge Data. *Journal of Hydrologic Engineering*, *11*(6), 555–569. doi.org/10.1061/(ASCE)1084-0699(2006)11:6(555)

Kang, M. S., Park, S. W., Lee, J. J., & Yoo, K. H. (2006). Applying SWAT for TMDL programs to a small watershed containing rice paddy fields. *Agricultural Water Management*, *79*(1), 72–92.

doi.org/10.1016/j.agwat.2005.02.015

Karizumi, N. (2010). *The latest illustrations of tree roots (Saishin jumoku konkei zusetsu)* (B5 ed.). Seibundo-shinkosha.

Kayaba, N., Yamada, T., Hayashi, S., Onogi, K., Kobayashi, S., Yoshimoto, K., Kamiguchi, K., & Yamashita, K. (2016). Dynamical Regional Downscaling Using the JRA-55 Reanalysis (DSJRA-55). *Sola*, *12*, 1–5. doi.org/10.2151/sola.2016-001

Kayitesi, N. M., Guzha, A. C., & Mariethoz, G. (2022). Impacts of land use land cover change and climate change on river hydro-morphology- a review of research studies in tropical regions. *Journal of Hydrology*, *615*, 128702. doi.org/10.1016/j.jhydrol.2022.128702

King, K. W., Arnold, J. G., & Bingner, R. (1999). Comparison of Green-Ampt and Curve Number Methods on Goodwin Creek Watershed Using SWAT. *Transactions of the ASABE (American Society of Agricultural and Biological Engineers)*, *42*(4), 919–926. doi.org/10.13031/2013.13272

Kingston, D. G., & Taylor, R. G. (2010). Sources of uncertainty in climate change impacts on river discharge and groundwater in a headwater catchment of the Upper Nile Basin, Uganda. *Hydrology and Earth System Sciences*, *14*(7), 1297–1308. doi.org/10.5194/hess-14-1297-2010

Kiros, G., Shetty, A., & Nandagiri, L. (2015). Performance Evaluation of SWAT Model for Land Use and Land Cover Changes in Semi-arid Climatic Conditions: A Review. *Hydrology Current Research*, *6*(3), 1000216. doi.org/10.4172/2157-7587.1000216

Knoben, W. J. M., Freer, J. E., & Woods, R. A. (2019). *Technical note: Inherent benchmark or not? Comparing Nash-Sutcliffe and Kling-Gupta efficiency scores* [Preprint]. Catchment hydrology/Modelling approaches. doi.org/10.5194/hess-2019-327

Kroll, C. N. (1989). *Estimation and usage of baseflow recession constants* [M.S. Thesis]. Tufts University.

Lahmer, W., Pfützner, B., & Becker, A. (2001). Assessment of land use and climate change impacts on the mesoscale. *Physics and Chemistry of the Earth, Part B: Hydrology, Oceans and Atmosphere*, *26*(7), 565–575. doi.org/10.1016/S1464-1909(01)00051-X

Li, H., Zhang, Y., Vaze, J., & Wang, B. (2012). Separating effects of vegetation change and climate variability using hydrological modelling and sensitivity-based approaches. *Journal of Hydrology*, *420–421*, 403–418. doi.org/10.1016/j.jhydrol.2011.12.033

Liu, J., & Lobb, D. (2021). An Overview of Crop and Crop Residue Management Impacts on Crop Water Use and Runoff in the Canadian Prairies. *Water*, *13*, 2929. doi.org/10.3390/w13202929

Liu, T., Amaya, T., Chaolun, B., & Liu, X. (2004). The Processes of Rainfall Infiltration and Phreatic Water Evaporation in Arid Area. *Transactions of The Japanese Society of Irrigation, Drainage and Reclamation Engineering*, *2004*(233), 449–460. doi.org/10.11408/jsidre1965.2004.449

Liu, Y., Xu, Y., Zhao, Y., & Long, Y. (2022). Using SWAT Model to Assess the Impacts of Land Use and Climate Changes on Flood in the Upper Weihe River, China. *Water*, *14*(13), Article 13. doi.org/10.3390/w14132098

López-Moreno, J. I., Begueria, S., & Garcia-Ruiz, J. M. (2006). Trends in high flows in the central Spanish Pyrenees: Response to climatic factors or to land-use change? *Hydrological Sciences Journal*, *51*(6), 1039–1050. doi.org/10.1623/hysj.51.6.1039

Ludwig, R., May, I., Turcotte, R., Vescovi, L., Braun, M., Cyr, J.-F., Fortin, L.-G., Chaumont, D., Biner, S., Chartier, I., Caya, D., & Mauser, W. (2009). The role of hydrological model complexity and uncertainty in climate change impact assessment. *Advances in Geosciences*, *21*, 63–71.

doi.org/10.5194/adgeo-21-63-2009

Maruyama, T. (1986). *Irrigation Draiage New Eddition (Shipen kangai haisui)*. Yokendo.

Mein, R. G., & Larson, C. L. (1973). Modeling infiltration during a steady rain. *Water Resources Research*, *9*(2), 384–394. doi.org/10.1029/WR009i002p00384

Mekonnen, M. A., Wörman, A., Dargahi, B., & Gebeyehu, A. (2009). Hydrological modelling of Ethiopian catchments using limited data. *Hydrological Processes*, *23*(23), 3401–3408. doi.org/10.1002/hyp.7470

Ministry of Internal Affairs and Communications. (2022). *Annual Population Estimated Reports*.

Miyabe, K., & Kudo, Y. (1986). *Field Guide on Major Trees in Hokkaido (Hokkaido shuyou jumoku zufu)*. Hokkaido University Press.

Miyata, S., Asaoka, Y., & Kazama, S. (2012). Verification of degree-day method and snowmelt rate factor in AMeDAS points over Japan. *Journal of Japan Society of Civil Engineers, Ser. B1 (Hydraulic Engineering)*, *68*(4), I_343-I_348. doi.org/10.2208/jscejhe.68.I_343

Mizuta, R., Yoshimura, H., Murakami, H., Matsueda, M., Endo, H., Ose, T., Kamiguchi, K., Hosaka, M., Sugi, M., Yukimoto, S., Kusunoki, S., & Kitoh, A. (2012). Climate Simulations Using MRI-AGCM3.2 with 20-km Grid. *Journal of the Meteorological Society of Japan. Ser. II*, *90A*, 233–258. doi.org/10.2151/jmsj.2012-A12

Mockus, V. (1972). National Engineering Handbook, Section 4 Hydrology. In *National Engineering Handbook*. USDA Natural Resources Conservation Service (former Soil Conservation Service).

Mori, K., & Sato, T. (2014). Spatio-Temporal Variation of High-Temperature Events in Hokkaido, North Japan. *Journal of the Meteorological Society of Japan. Ser. II*, *92*(4), 327–346. doi.org/10.2151/jmsj.2014-404

Mulungu, D. M. M., & Munishi, S. E. (2007). Simiyu River catchment parameterization using SWAT model. *Physics and Chemistry of the Earth, Parts A/B/C*, *32*(15), 1032–1039. doi.org/10.1016/j.pce.2007.07.053

Musiake, K., Takahasi, Y., & Ando, Y. (1981). Effects of Basin Geology on River-Flow Regime in Mountainous Areas of Japan. *Proceedings of the Japan Society of Civil Engineers*, *1981*(309), 51–62. doi.org/10.2208/jscej1969.1981.309_51

Myneni, R., Knyazikhin, Y., & Park, T. (2015). *MOD15A2H MODIS Leaf Area Index/FPAR 8-Day L4 Global 500m SIN Grid V006.* [Terra]. doi.org/10.5067/MODIS/MOD15A2H.006

Nakagawa, S. (1966). Water requirement survey and planning act in paddy field (Suiden yousuiryo chosa keikakuhou). *Journal of the Agricultural Engineering Society, Japan*, *34*(1, 2, 6, 9, 10, 11, 12). doi.org/10.11408/jjsidre1965.34.25

Nakajima, Y., Shimizu, H., Ogawa, N. O., Sakamoto, T., Okada, H., Koba, K., Kitazato, H., & Ohkouchi, N. (2004). Vertical distributions of stable isotopic compositions and bacteriochlorophyll homologues in suspended particulate matter in saline meromictic Lake Abashiri. *Limnology*, *5*(3), 185–189. doi.org/10.1007/s10201-004-0125-6

Nakatsugawa, M. (2015). *Adaptation measures to global warming that should be considered in Hokkaido* (Docon Report, pp. 2–7). Muroran Institute of Technology.

Nash, J. E., & Sutcliffe, J. V. (1970). River flow forecasting through conceptual models part I — A discussion of principles. *Journal of Hydrology*, *10*(3), 282–290. doi.org/10.1016/0022-1694(70)90255-6

Neitsch, S. L., Arnold, J. G., Kiniry, J. R., & Williams, J. R. (2011). *Soil and Water Assessment Tool Theoretical Documentation Version 2009* [Technical Report]. Texas Water Resources Institute.

Nur Syahida, A. M., & Azinoor Azida, A. B. (2018). The effect of vegetation canopy on canopy storage capacity with different rainfall intensity. *MATEC Web of Conferences*, *250*, 04001. doi.org/10.1051/matecconf/201825004001

Obara, H., Ohkura, T., Takata, Y., Kohyama, K., Maejima, Y., & Hamazaki, T. (2011). *Comprehensive Soil Classification System of Japan First Approximation* (No. 29; p. 73). National Institute for Agro-Environmental Sciences.

Odani, H. (2015). Relationship between Actual Evapotranspiration and Potential Evapotranspiration Calculated by the Equation Simplified from the FAO Penman-Monteith Equation in a Paddy Field. *Transactions of The Japanese Society of Irrigation, Drainage and Rural Engineering*, *83*(3), I_73-I_81. doi.org/10.11408/jsidre.83.I_73

Ogawa, M., Takenaka, A., Kadoya, T., Ishihama, F., Yamano, H., & Akasaka, M. (2013). A comprehensive new land-use classification map for Japan for biodiversity assessment and species distribution modeling. *Japanese Journal of Conservation Ecology*, *18*(1), 69–76. doi.org/10.18960/hozen.18.1_69

Ritter, A., & Muñoz-Carpena, R. (2013). Performance evaluation of hydrological models: Statistical significance for reducing subjectivity in goodness-of-fit assessments. *Journal of Hydrology*, *480*, 33–45. doi.org/10.1016/j.jhydrol.2012.12.004

Saito, K., Fujita, T., Yamada, Y., Ishida, J., Kumagai, Y., Aranami, K., Ohmori, S., Nagasawa, R., Kumagai, S., Muroi, C., Kato, T., Eito, H., & Yamazaki, Y. (2006). The Operational JMA Nonhydrostatic Mesoscale Model. *Monthly Weather Review*, *134*(4), 1266–1298. doi.org/10.1175/MWR3120.1

Saito, O., Kamiyama, C., Hashimoto, S., Matsui, T., Shoyama, K., Kabaya, K., Uetake, T., Taki, H., Ishikawa, Y., Matsushita, K., Yamane, F., Hori, J., Ariga, T., & Takeuchi, K. (2019). Co-design of national-scale future scenarios in Japan to predict and assess natural capital and ecosystem services. *Sustainability Science*, *14*(1), 5–21. doi.org/10.1007/s11625-018-0587-9

Sakaguchi, A., Eguchi, S., Kato, T., Kasuya, M., Ono, K., Miyata, A., & Tase, N. (2014). Development and evaluation of a paddy module for improving hydrological simulation in SWAT. *Agricultural Water Management*, *137*, 116–122. doi.org/10.1016/j.agwat.2014.01.009

Sakai T. (1963). A study of the snow-melt runoff of rivers. *Transactions of the Japan Society of Civil Engineers*, *1963*(95), 9–20. doi.org/10.2208/jscej1949.1963.95_9

Sakata, Y., Uehara, H., Chikita, K. A., Nakatsugawa, M., Yamada, T. J., Kudo, K., & Usutani, T. (2016). Regional Regression Analysis of Drought River Discharges in Snowy Cold Areas Under Climate Change. *Journal of Japan Society of Civil Engineers, Ser. G (Environmental Research)*, *72*(5), I_253-I_264. doi.org/10.2208/jscejer.72.I_253

Sasaki, H., Murata, A., Hanafusa, M., Oh'izumi, M., & Kurihara, K. (2011). Reproducibility of Present Climate in a Non-Hydrostatic Regional Climate Model Nested within an Atmosphere General Circulation Model. *Sola*, *7*, 173–176. doi.org/10.2151/sola.2011-044

Sato, M. (2014). *Remote Sensing in Forest, from Fundamentals to Applications* (4th edition). Japan Forestry Investigation Committie.

Schilling, K. E., Jha, M. K., Zhang, Y.-K., Gassman, P. W., & Wolter, C. F. (2008). Impact of land use and land cover change on the water balance of a large agricultural watershed: Historical effects and future directions. *Water Resources Research*, *44*(7). doi.org/10.1029/2007WR006644

Setegn, S. G., Srinivasan, R., & Dargahi, B. (2008). Hydrological Modelling in the Lake Tana Basin, Ethiopia Using SWAT Model. *The Open Hydrology Journal*, *2*(1).

Sheffield, J., & Wood, E. F. (2011). *Drought: Past Problems and Future Scenarios* (1st ed.). Routledge, U.K. doi.org/10.4324/9781849775250

Shi, M., Shiraiwa, T., Mitsudera, H., & Muravyev, Y. (2021). Estimation of freshwater discharge from the Kamchatka Peninsula to its surrounding oceans. *Journal of Hydrology: Regional Studies*, *36*, 100836. doi.org/10.1016/j.ejrh.2021.100836

Shimizu, Y., Onodera, S., & Saito, M. (2013). Applicability of SWAT Model for Estimation of Phosphorus Discharge in a Suburban Catchment. *Journal of Japan Society of Hydrology and Water Resources*, *26*(3), 153–173. doi.org/10.3178/jjshwr.26.153

Shoyama, K. (2021). Assessment of Land-Use Scenarios at a National Scale Using Intensity Analysis and Figure of Merit Components. *Land*, *10*(4), Article 4. doi.org/10.3390/land10040379

Shoyama, K., Matsui, T., Hashimoto, S., Kabaya, K., Oono, A., & Saito, O. (2019). Development of land-use scenarios using vegetation inventories in Japan. *Sustainability Science*, *14*(1), 39–52. doi.org/10.1007/s11625-018-0617-7

Sivapalan, M. (2003). Process complexity at hillslope scale, process simplicity at the watershed scale: Is there a connection? *Hydrological Processes*, *17*(5), 1037–1041. doi.org/10.1002/hyp.5109

Spilling, K. H. (2018). *Pedotransfer functions for predicting hydraulic properties of non-allophanic andosols and histosols in the páramo of Southern Ecuador* [Norwegian University of Life Sciences].

Strauch, M., & Volk, M. (2013). SWAT plant growth modification for improved modeling of perennial vegetation in the tropics. *Ecological Modelling*, *269*, 98–112. doi.org/10.1016/j.ecolmodel.2013.08.013

Sugihara, K., & Hirai, Y. (2015). Relationship Between Corbicula Japonica Habitat and Flow Regime

Change Based on Water Balance of Sarobetsu River. *Journal of Japan Society of Civil Engineers, Ser. G (Environmental Research)*, *71*(5), I_79-I_86. doi.org/10.2208/jscejer.71.I_79

Sugimoto, S., Sato, T., & Sasaki, T. (2015a). Impact of Land-Use Change on Winter Precipitation in Hokkaido, Japan. *Sola*, *11*, 95–99. doi.org/10.2151/sola.2015-023

Sugimoto, S., Sato, T., & Sasaki, T. (2015b). Seasonal and diurnal variability in historical warming due to the urbanization of Hokkaido, Japan. *Journal of Geophysical Research: Atmospheres*, *120*(11), 5437–5445. doi.org/10.1002/2014JD022759

Tachikawa, Y., Takino, S., Fujioka, Y., Yorozu, K., Kim, S., & Shiiba, M. (2011). Projection of River Discharge of Japanese River Basins Under a Climate Change Scenario. *Journal of Japan Society of Civil Engineers, Ser. B1 (Hydraulic Engineering)*, *67*(1), 1–15. doi.org/10.2208 /jscejhe.67.1

Tan, X., & Gan, T. Y. (2015). Contribution of human and climate change impacts to changes in streamflow of Canada. *Scientific Reports*, *5*(1), Article 1. doi.org/10.1038/srep17767

Tao, B., Tian, H., Ren, W., Yang, J., Yang, Q., He, R., Cai, W., & Lohrenz, S. (2014). Increasing Mississippi river discharge throughout the 21st century influenced by changes in climate, land use, and atmospheric CO2. *Geophysical Research Letters*, *41*(14), 4978–4986. doi.org/10.1002/2014GL060361

Tasdighi, A., Arabi, M., & Harmel, D. (2018). A probabilistic appraisal of rainfall-runoff modeling approaches within SWAT in mixed land use watersheds. *Journal of Hydrology*, *564*, 476–489. doi.org/10.1016/j.jhydrol.2018.07.035

Tibebe, D., & Bewket, W. (2011). Surface runoff and soil erosion estimation using the SWAT model in the Keleta Watershed, Ethiopia. *Land Degradation & Development*, *22*(6), 551–564.

doi.org/10.1002/ldr.1034

Tolson, B. A., & Shoemaker, C. A. (2007). Cannonsville Reservoir Watershed SWAT2000 model development, calibration and validation. *Journal of Hydrology*, *337*(1), 68–86. doi.org/10.1016/j.jhydrol.2007.01.017

Tsuchiya, R., Kato, T., Jeong, J., & Arnold, J. G. (2018). Development of SWAT-Paddy for Simulating Lowland Paddy Fields. *Sustainability*, *10*(9), Article 9. doi.org/10.3390/su10093246

Turner, B. L., Skole, D., Sanderson, S., Fischer, G., Fresco, L., & Leemans, R. (1995). Land-Use and Land-Cover Change: Science/research plan. *Scanning Electron Microscopy*.

Twine, T. E., Kucharik, C. J., & Foley, J. A. (2004). Effects of Land Cover Change on the Energy and Water Balance of the Mississippi River Basin. *Journal of Hydrometeorology*, *5*(4), 640–655. doi.org/10.1175/1525-7541(2004)005<0640:EOLCCO>2.0.CO;2

Usutani, T., & Nakatsugawa, M. (2005). Winter Warming Trends and Their Effect's on the Hydrologic Cycle in Hokkaido. *Proceedings of the Symposium on Global Environment*, *13*, 1–6. doi.org/10.2208/proge.13.1

Utoh, H. (1981). Growth of the brackish-water bivalve, Corbicula japonica PRIME, in Lake Abashiri. *Scientific Reports of Hokkaido Fisheries Research Institutes*, *23*, 65–81.

van Griensven, A., Meixner, T., Grunwald, S., Bishop, T., Diluzio, M., & Srinivasan, R. (2006). A global sensitivity analysis tool for the parameters of multi-variable catchment models. *Journal of Hydrology*, *324*(1), 10–23. doi.org/10.1016/j.jhydrol.2005.09.008

van Griensven, A., Ndomba, P., Yalew, S., & Kilonzo, F. (2012). Critical review of SWAT applications in the upper Nile basin countries. *Hydrology and Earth System Sciences*, *16*(9), 3371–3381. doi.org/10.5194/hess-16-3371-2012 van Vliet, M. T. H., Franssen, W. H. P., Yearsley, J. R., Ludwig, F., Haddeland, I., Lettenmaier, D. P., & Kabat, P. (2013). Global river discharge and water temperature under climate change. *Global Environmental Change*, *23*(2), 450–464. doi.org/10.1016/j.gloenvcha.2012.11.002

Vogel, R. M., & Kroll, C. N. (1996). Estimation of baseflow recession constants. *Water Resources Management*, *10*(4), 303–320. doi.org/10.1007/BF00508898

Wang, F., Ge, Q., Yu, Q., Wang, H., & Xu, X. (2017). Impacts of land-use and land-cover changes on river runoff in Yellow River basin for period of 1956–2012. *Chinese Geographical Science*, *27*(1), 13–24. doi.org/10.1007/s11769-017-0843-3

Wang, S., McVicar, T. R., Zhang, Z., Brunner, T., & Strauss, P. (2020). Globally partitioning the simultaneous impacts of climate-induced and human-induced changes on catchment streamflow: A review and meta-analysis. *Journal of Hydrology*, *590*, 125387. doi.org/10.1016/j.jhydrol.2020.125387

Ward, P. J., Renssen, H., Aerts, J. C. J. H., van Balen, R. T., & Vandenberghe, J. (2008). Strong increases in flood frequency and discharge of the River Meuse over the late Holocene: Impacts of long-term anthropogenic land use change and climate variability. *Hydrology and Earth System Sciences*, *12*(1), 159–175. doi.org/10.5194/hess-12-159-2008

Watanabe, T., Miyakoshi, Y., Mano, S., Kawajiri, T., Suezawa, K., & Hayano, H. (2021). Growth and age to catchable size of brackish water bivalve *Corbicula japonica* in Lake Abashiri, Hokkaido, Japan. *Nippon Suisan Gakkaishi*, *87*(2), 132–143. doi.org/10.2331/suisan.20-00007

Wijesekara, G. N., Gupta, A., Valeo, C., Hasbani, J.-G., Qiao, Y., Delaney, P., & Marceau, D. J. (2012). Assessing the impact of future land-use changes on hydrological processes in the Elbow River watershed in southern Alberta, Canada. *Journal of Hydrology*, *412–413*, 220–232.

doi.org/10.1016/j.jhydrol.2011.04.018

Williams, J. R., Arnold, J. G., Kiniry, J. R., Gassman, P. W., & Green, C. H. (2008). History of model development at Temple, Texas. *Hydrological Sciences Journal*, *53*(5), 948–960. doi.org/10.1623/hysj.53.5.948

Xiao, Q., & McPherson, E. G. (2016). Surface Water Storage Capacity of Twenty Tree Species in Davis, California. *Journal of Environmental Quality*, *45*(1), 188–198. doi.org/10.2134/jeq2015.02.0092

Yu, K., Pypker, T., Keim, R., Chen, N., Yingbo, Y., Guo, S., Li, W., & Wang, G. (2012). Canopy rainfall storage capacity as affected by sub-alpine grassland degradation in the Qinghai-Tibetan Plateau, China. *Hydrological Processes*, *26*, 3114–3123. doi.org/10.1002/hyp.8377

Zhang, H., Wang, B., Liu, D. L., Zhang, M., Leslie, L. M., & Yu, Q. (2020). Using an improved SWAT model to simulate hydrological responses to land use change: A case study of a catchment in tropical Australia. *Journal of Hydrology*, *585*, 124822. doi.org/10.1016/j.jhydrol.2020.124822

Zhao, F., Zhang, L., Xu, Z., & Scott, D. F. (2010). Evaluation of methods for estimating the effects of vegetation change and climate variability on streamflow. *Water Resources Research*, *46*(3). doi.org/10.1029/2009WR007702

Zheng, J., Sun, G., Li, W., Yu, X., Zhang, C., Gong, Y., & Tu, L. (2016). Impacts of land use change and climate variations on annual inflow into the Miyun Reservoir, Beijing, China. *Hydrology and Earth System Sciences*, *20*(4), 1561–1572. doi.org/10.5194/hess-20-1561-2016

Zou, C., Caterina, G., Will, R., Stebler, E., & Turton, D. (2015). Canopy Interception for a Tallgrass Prairie under Juniper Encroachment. *PloS One*, *10*, e0141422. doi.org/10.1371/journal.pone.0141422